Magnetic Feshbach resonances in ultracold collisions between Cs and Yb atoms

B. C. Yang,[1] Matthew D. Frye,[1] A. Guttridge,[2] Jesus Aldegunde,[3] Piotr S. Żuchowski,[4] Simon L. Cornish,[2,*] and Jeremy M. Hutson[1,†]

[1]*Joint Quantum Centre (JQC) Durham-Newcastle, Department of Chemistry, Durham University, South Road, Durham DH1 3LE, United Kingdom*

[2]*Joint Quantum Centre (JQC) Durham-Newcastle, Department of Physics, Durham University, South Road, Durham DH1 3LE, United Kingdom*

[3]*Departamento de Quimica Fisica, Universidad de Salamanca, 37008 Salamanca, Spain*

[4]*Institute of Physics, Faculty of Physics, Astronomy and Informatics, Nicolaus Copernicus University, Grudziadzka 5/7, 87-100 Torun, Poland*

(Received 28 May 2019; published 15 August 2019)

We investigate magnetically tunable Feshbach resonances in ultracold collisions between ground-state Yb and Cs atoms, using coupled-channel calculations based on an interaction potential recently determined from photoassociation spectroscopy. We predict resonance positions and widths for all stable isotopes of Yb, together with resonance decay parameters where appropriate. The resonance patterns are richer and more complicated for fermionic Yb than for spin-zero isotopes, because there are additional level splittings and couplings due to scalar and tensorial Yb hyperfine interactions. We examine collisions involving Cs atoms in a variety of hyperfine states and identify resonances that appear most promising for experimental observation and for magnetoassociation to form ultracold CsYb molecules.

DOI: 10.1103/PhysRevA.100.022704

I. INTRODUCTION

Magnetic Feshbach resonances are a valuable tool for tuning the scattering length by varying an external magnetic field and have found a wide range of applications in the study and control of ultracold gases [1]. Great progress has been achieved in the exploration of Feshbach resonances for pairs of alkali-metal atoms. One significant achievement is the formation of ultracold molecules by adiabatically ramping the magnetic field across a zero-energy Feshbach resonance [2–10], known as magnetoassociation [11,12]. The resulting weakly bound dimers can be transferred to their absolute ground states by stimulated Raman adiabatic passage [13–20]. These ultracold molecules promise diverse applications in fields from ultracold chemistry to precision measurement, due to their rich internal degrees of freedom and complex interactions compared to ultracold atoms [21,22]. In particular, the inherent electric dipole moment of ultracold polar molecules makes them valuable in the study of quantum dipolar matter [23,24] and for applications in quantum computation and simulation [25,26].

There is currently great interest in ultracold mixtures of alkali-metal and closed-shell (^1S) atoms [27–38]. The molecules formed from these atoms have $^2\Sigma$ ground states with unpaired electron spin. They therefore have both electric and magnetic dipole moments and provide a platform for studying lattice spin models in many-body physics [39]. They may also be valuable in searches for the electric dipole moment of the electron [40]. However, magnetoassociation in such mixtures will be challenging because the Feshbach resonances are expected to be narrow. This is because the lack of structure of a ^1S atom removes the strong couplings that cause many wide resonances in alkali + alkali systems; the strongest source of coupling in alkali + ^1S systems is the weak dependence of hyperfine coupling on interatomic distance [32,33]. Nevertheless, Feshbach resonances have recently been observed in an ultracold Rb + Sr mixture [41]. There is now great hope that it will be possible to form ultracold open-shell molecules by magnetoassociation at these resonances.

We have studied ultracold Cs + Yb mixtures both experimentally and theoretically [34,36–38,42]. The merits of this system include the existence of seven stable isotopes of Yb, including five spin-zero bosons and two fermions. Because of the large mass of Cs, significant variation of the atom-pair reduced mass can be achieved by choosing different isotopes of Yb. This produces a wide variety of Feshbach resonances with substantially different properties for different isotopes [34]. However, the predictions of Ref. [34] were limited because, at that time, the ground-state interaction potential was not known accurately enough to predict scattering lengths for specific isotopic combinations.

In recent work, we have measured the binding energies of near-threshold bound states for several isotopologs of CsYb and determined the ground-state electronic potential [43]. This allows us to make specific predictions for the positions and widths of Feshbach resonances. Figure 1 shows the atomic thresholds for Cs as a function of magnetic field and the near-threshold energy levels of CsYb predicted for the ground-state potential of Ref. [43]. Because there is only a single

*s.l.cornish@durham.ac.uk
†j.m.hutson@durham.ac.uk

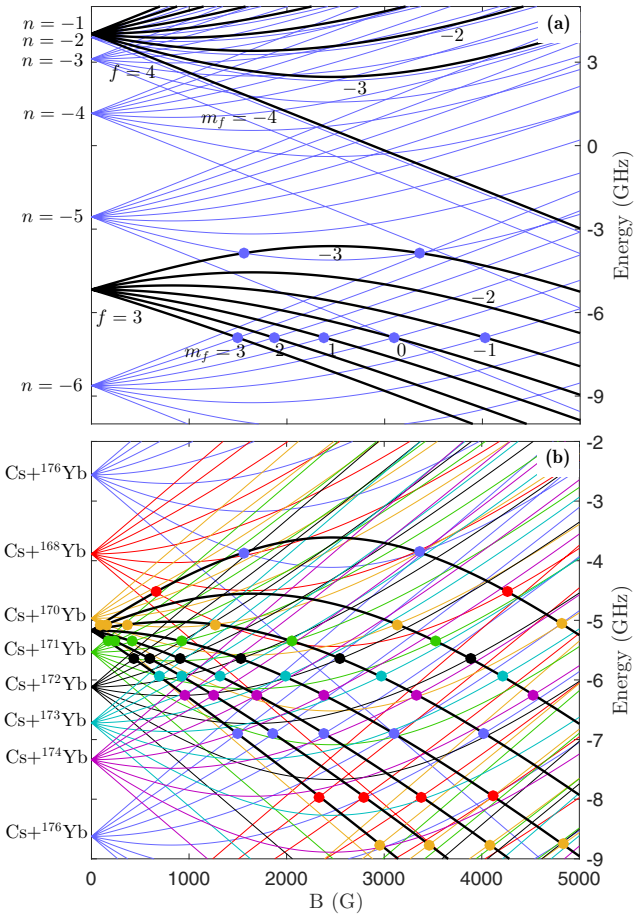

FIG. 1. Near-threshold bound states (thin colored lines) crossing atomic thresholds (thick black lines) as a function of magnetic field. The solid circles mark the Feshbach resonances caused by the dependence of the Cs hyperfine coupling on the internuclear distance. (a) The hyperfine + Zeeman splittings of the atomic thresholds and molecular bound states for the example of Cs + ^{176}Yb. The atomic levels are labeled by quantum numbers f and m_f as discussed in the text. Only molecular levels from the upper hyperfine manifold ($f = 4$) are shown, labeled by the vibrational number n. (b) Molecular levels for $n = -5$ and -6 for all isotopic combinations, with Feshbach resonance positions at crossings with atomic states in the lower hyperfine manifold.

electronic state and the hyperfine coupling is weakly dependent on distance, the full molecular states are essentially single channel in nature; they have the same spin character as the threshold that supports them and run parallel to it as a function of magnetic field [32,34]. Feshbach resonances due to the Cs hyperfine coupling are predicted at the crossings indicated by colored dots. The figure also shows how different choices of Yb isotope shift the near-threshold states and strongly affect the resonance positions.

In this paper, we perform coupled-channel calculations to identify, locate, and characterize Feshbach resonances in ultracold collisions between Cs and Yb atoms. Our main focus is to understand the physics behind the properties of Feshbach resonances in this system and to establish which Feshbach resonances are promising for experimental observation and molecule formation. In Sec. II, we introduce the underlying theory of these Feshbach resonances: the coupling terms in the Hamiltonian which cause them, the methods we use to characterize them, and the framework we use to understand the results. In Sec. III, we use Cs + ^{173}Yb as an example system to discuss the effects of the different coupling mechanisms and the general characteristics of the different resonances they cause. In Sec. IV, we identify promising resonances for observation and magnetoassociation for various isotopic combinations of Cs + Yb, taking account of experimental considerations. Comprehensive results for resonances of all isotopic combinations are provided in Supplemental Material [44].

II. THEORETICAL BACKGROUND

We consider the ultracold scattering between ^{133}Cs(^2S) and Yb(^1S) atoms. The Hamiltonian $\hat{H}$ can be written [33]

$$\hat{H} = \frac{\hbar^2}{2\mu}\left[-\frac{1}{R}\frac{d^2}{dR^2}R + \frac{\hat{L}^2}{R^2}\right] + \hat{H}_{\rm Cs} + \hat{H}_{\rm Yb} + \hat{U}(R), \quad (1)$$

where R is the internuclear distance, μ is the reduced mass, and $\hbar$ is the reduced Planck constant. $\hat{L}$ is the two-atom rotational angular momentum operator, with quantum number L and projection M_L. $\hat{H}_{\rm Cs}$ and $\hat{H}_{\rm Yb}$ are the Hamiltonians for the separated single atoms, which are independent of R and contain hyperfine coupling and Zeeman terms,

$$\hat{H}_{\rm Cs} = \zeta_{\rm Cs}\hat{i}_{\rm Cs}\cdot\hat{s} + (g_{\rm Cs}\hat{i}_{{\rm Cs},z} + g_s\hat{s}_z)\mu_{\rm B}B, \quad (2)$$

$$\hat{H}_{\rm Yb} = g_{\rm Yb}\hat{i}_{{\rm Yb},z}\mu_{\rm B}B. \quad (3)$$

Here, B is a magnetic field oriented along the z axis, and $\mu_{\rm B}$ is the Bohr magneton. $\zeta_{\rm Cs}$ is the hyperfine coupling constant for the Cs atom. $\hat{i}_{\rm Cs}$, $\hat{i}_{\rm Yb}$, and $\hat{s}$ are the nuclear and electron spin operators, with projections on the z axis $\hat{i}_{{\rm Cs},z}$, $\hat{i}_{{\rm Yb},z}$, and $\hat{s}_z$; their corresponding g factors are $g_{\rm Cs}$, $g_{\rm Yb}$, and g_s, respectively. The specific values of $\zeta_{\rm Cs}$, $g_{\rm Cs}$, and g_s in this work are taken from Ref. [45] and those for $g_{\rm Yb}$ are obtained from the shielded magnetic moments (without diamagnetic correction) of Ref. [46].

The interaction operator $\hat{U}(R)$ is divided into the electronic interaction potential $V_{\rm elec}(R)$ and spin-dependent terms $\hat{V}_{\rm spin}(R)$. The electronic potential is by far the strongest interaction and almost completely determines the bound states and nonresonant scattering in each channel. However, it cannot change the electron or nuclear spins and so does not couple different channels or cause Feshbach resonances. We use the ground-state interaction potential fitted to two-photon spectroscopy in Ref. [43], which provides an accurate representation of the near-threshold bound states that produce Feshbach resonances. This potential was fitted without including the contribution of the spin-dependent terms. However, the shifts due to these terms are only a few MHz even for the deepest states measured in Ref. [43] and are much smaller for the shallower states that are important in the present work. The scattering length and the binding energy of the highest bound state are given in Table I for Cs interacting with each isotope of Yb on this potential (without any internal structure on either collision partner).

TABLE I. Scattering length and binding energy of the highest bound state for Cs interacting with each isotope of Yb on the potential $V_{\rm elec}(R)$ of Ref. [43].

Mixture	a (units of a_0)	$E_{\rm b}(n=-1)/h$ (MHz)
Cs + ^{168}Yb	165.98	3.70
Cs + ^{170}Yb	96.24	15.6
Cs + ^{171}Yb	69.99	25.8
Cs + ^{172}Yb	41.03	39.5
Cs + ^{173}Yb	1.0	57.0
Cs + ^{174}Yb	−74.8	78.7
Cs + ^{176}Yb	798	0.0513

A. Spin-dependent terms

The systems considered here lack the strong couplings that cause wide Feshbach resonances for pairs of alkali-metal atoms, due to differences between singlet and triplet potentials and electron spin-spin couplings. Instead, couplings between different channels are caused by the change in hyperfine interactions due to the proximity of the two atoms. The operator $\hat{V}_{\rm spin}(R)$ may be written as [47]

$$\begin{aligned}\hat{V}_{\rm spin}(R) = {}& \Delta\zeta_{\rm Cs}(R)\hat{i}_{\rm Cs}\cdot\hat{s} + \Delta\zeta_{\rm Yb}(R)\hat{i}_{\rm Yb}\cdot\hat{s} \\ & + t_{\rm Yb}(R)\sqrt{6}\,T^2(\hat{i}_{\rm Yb},\hat{s})\cdot T^2(C) \\ & + t_{\rm Cs}(R)\sqrt{6}\,T^2(\hat{i}_{\rm Cs},\hat{s})\cdot T^2(C) \\ & + e\boldsymbol{Q}_{\rm Yb}\cdot\boldsymbol{q}_{\rm Yb}(R) \\ & + e\boldsymbol{Q}_{\rm Cs}\cdot\boldsymbol{q}_{\rm Cs}(R) + \gamma(R)\hat{s}\cdot\hat{L}. \end{aligned} \quad (4)$$

The first two terms represent the scalar contact interaction between the electron and nuclear spins, while the third and fourth terms represent the corresponding dipolar interaction. Here, T^2 indicates a spherical tensor of rank 2; $T^2(C)$ has components $C^2_q(\theta,\phi)$, where C is a renormalized spherical harmonic and θ, ϕ are the polar coordinates of the internuclear vector. The fifth and sixth terms represent the interaction between the nuclear electric quadrupole tensor $e\boldsymbol{Q}_j$ of nucleus j and the distance-dependent electric field gradient tensor $\boldsymbol{q}_j(R)$ at the nucleus, due to the electrons. The final term represents the interaction between the electron spin and the molecular rotation.

The first three terms in Eq. (4) are the ones that are principally responsible for Feshbach resonances in CsYb and similar systems. We refer to them as mechanisms I, II, and III, respectively; each can be written as the product of a purely R-dependent term $\omega_x(R)$ and a purely spin-dependent term $\hat{\Omega}_x$ that is different for each of x = I, II, and III.

Mechanism I is due to the variation in hyperfine coupling on the Cs atom, $\hat{\Omega}_{\rm I} = \hat{i}_{\rm Cs}\cdot\hat{s}$. This arises because the approaching Yb atom pulls electron-spin density away from the Cs nucleus, thereby reducing the strength of the hyperfine interaction. This coupling mechanism was first proposed by Żuchowski *et al.* [32] for Rb + Sr and was investigated extensively by Brue and Hutson for alkali-metal + Yb systems [34]. As it relies only on the Cs nuclear spin, it exists for all isotopic combinations of Cs + Yb.

Mechanism II is due to the variation in hyperfine coupling on the Yb atom, $\hat{\Omega}_{\rm II} = \hat{i}_{\rm Yb}\cdot\hat{s}$. This mechanism is complementary to mechanism I: As electron-spin density is pulled away from the Cs nucleus, some of it comes into contact with the Yb nucleus, where it can interact with a nuclear spin. This mechanism was first proposed by Brue and Hutson [33]. It exists only for Yb isotopes with a nonzero nuclear spin, so only for ^{171}Yb and ^{173}Yb.

Mechanism III is due to the tensor, or anisotropic, hyperfine coupling on the Yb atom, $\hat{\Omega}_{\rm III} = \sqrt{6}T^2(\hat{i}_{\rm Yb},\hat{s})\cdot T^2(C)$. The approach of the Cs atom breaks the spherical symmetry of the electron density around the Yb nucleus and allows a dipolar coupling that can cause resonances due to $L=2$ bound states in s-wave scattering. This mechanism was briefly considered by Brue and Hutson [33] but they ultimately neglected it; nevertheless, resonances caused by this mechanism were later observed in Rb + ^{87}Sr [41]. Like mechanism II, this mechanism relies on the Yb nuclear spin so exists only for ^{171}Yb and ^{173}Yb.

The fourth term in Eq. (4), involving $t_{\rm Cs}$, is analogous to the third term and may formally be considered as contributing to mechanism III. However, it is very weak in CsYb, as discussed below. The quadrupole term involving $Q_{\rm Yb}$ does not generally produce resonances but may cause significant level shifts for levels of Cs^{171}Yb and Cs^{173}Yb with $L>0$, as described in Sec. III C. The quadrupole term involving $Q_{\rm Cs}$ can in principle cause resonances due to $L=2$ bound states but is very weak in CsYb. The spin-rotation term $\gamma(R)\hat{s}\cdot\hat{L}$ has no matrix elements involving $L=0$ states and so does not cause resonances in s-wave scattering. All terms except that involving $t_{\rm Cs}$ are included where applicable in the coupled-channel calculations described below.

B. Electronic structure calculations of spin-dependent coefficients

We have calculated values of the scalar hyperfine coupling coefficients $\zeta_{\rm Cs}(R)$ and $\zeta_{\rm Yb}(R)$, the corresponding tensor coefficients $t_{\rm Cs}(R)$ and $t_{\rm Yb}(R)$, and the nuclear quadrupole coupling coefficients $(eQq)_{\rm Cs}(R)$ and $(eQq)_{\rm Yb}(R)$. We have also calculated the electron g-tensor anisotropy $\Delta g_\perp(R)$, which is related to the spin-rotation coefficient $\gamma(R)$ [47]. We carried out density-functional (DFT) calculations using the Amsterdam density functional (ADF) package [48,49] as described in Ref. [47], at 40 distances from $R=3.8$ Å to 20 Å. The coefficients for ^{171}Yb are obtained from those for ^{173}Yb by scaling using nuclear g factors, nuclear quadrupole moments, and molecular rotational constants as described in Ref. [50].

Aldegunde and Hutson [47] concluded that the B3LYP functional [51,52] gives good accuracy for hyperfine coupling coefficients in $^2\Sigma$ molecules and that spin-unrestricted calculations are slightly more accurate than restricted calculations when the two results are similar. We obtained similar results from restricted and unrestricted calculations, so we report the unrestricted results here. The one exception to this is the coefficient $t_{\rm Cs}(R)$, which is so small that the differences between the restricted and unrestricted results are comparable to their absolute magnitude. We consider these results to be consistent with zero, so we do not report $t_{\rm Cs}(R)$ and exclude the corresponding term from our coupled-channel calculations.

TABLE II. Parameters for the R dependence of the spin-dependent coefficients.

	A_0 (MHz)	a (Å^{-2})	R_c (Å)	b (Å^{-1})	σ_0 (Å)
$\Delta\zeta$ (^{133}Cs)	−241	0.154	3.33	–	–
$\Delta\zeta$ (^{173}Yb)	−126	0.144	3.42	–	–
$\Delta\zeta$ (^{171}Yb)	457	0.144	3.42	–	–
eQq (^{133}Cs)	0.227	0.256	3.28	–	–
eQq (^{173}Yb)	−601	0.249	3.32	–	–
t (^{173}Yb)	−24.5	–	–	0.953	4.1
t (^{171}Yb)	88.9	–	–	0.953	4.1
γ	21.7	–	–	1.58	4.1

For all the coefficients, the values from DFT calculations behave irregularly inside the zero-energy inner turning point σ_0, which is at 4.1 Å for CsYb. The irregularities probably occur because different electronic states mix strongly in the region of the repulsive wall. Since the resonance properties of interest here are insensitive to the behavior of the couplings inside the inner turning point, we have fitted functional forms to the points at $R \geqslant 4.0$ Å.

The scalar hyperfine coupling coefficients $\Delta\zeta_{\rm Cs}(R) = \zeta_{\rm Cs}(R) - \zeta_{\rm Cs}$ and $\Delta\zeta_{\rm Yb}(R) = \zeta_{\rm Yb}(R)$ are both negative for all $R > \sigma_0$, but both of them show positive curvature slightly outside σ_0. The same is true for the quadrupole coupling coefficients $(eQq)_{\rm Cs}(R)$ and $(eQq)_{\rm Yb}(R)$. For consistency with Brue and Hutson [34], we have chosen to represent these coefficients with Gaussian functions, $A_0 \exp[-a(R - R_c)^2]$. However, there is no sign of such curvature for $t_{\rm Yb}$ or $\gamma(R)$, and for these we have used simple decaying exponentials $A_0 \exp[-b(R - \sigma_0)]$, with σ_0 fixed at 4.1 Å. The resulting parameters are given in Table II.

The calculated function $\Delta\zeta_{\rm Cs}(R)$ predicts that the $f = 4$, $n = -7$ level of Cs ^{174}Yb is bound by 11 MHz more than the corresponding $f = 3$ level. This may be compared with an experimental shift of 10 ± 3 MHz from two-photon photoassociation spectroscopy [43,53].

C. Magnetic Feshbach resonances

A magnetic Feshbach resonance occurs when a molecular bound state is tuned across an atomic scattering threshold by varying an applied magnetic field. For an isolated resonance without inelastic decay, the scattering length $a(B)$ has a characteristic pole at the resonance position $B_{\rm res}$ [54],

$$a(B) = a_{\rm bg}\left(1 - \frac{\Delta}{B - B_{\rm res}}\right), \tag{5}$$

where $a_{\rm bg}$ is the background scattering length. The resonance width Δ can be artificially large if $a_{\rm bg}$ is particularly small. A better measure of the strength of the resonant pole is the product $a_{\rm bg}\Delta$, which provides a measure of the observability of the resonance in three-body loss spectroscopy and is proportional to the rate of the field sweep needed to achieve adiabatic passage in magnetoassociation [55,56]. However, $a_{\rm bg}\Delta$ has inconvenient dimensions for qualitative discussion; in order to maintain a measure with dimensions of magnetic field, we define a normalized width

$$\bar{\Delta} = a_{\rm bg}\Delta/\bar{a}, \tag{6}$$

where $\bar{a} = (2\mu C_6/\hbar^2)^{1/4} \times 0.4779888\ldots$ is the mean scattering length of Gribakin and Flambaum [57] and ranges from 83.62 a_0 for Cs + ^{168}Yb to 84.05 a_0 for Cs + ^{176}Yb.

When inelastic decay occurs, the scattering length becomes complex, with the imaginary part describing inelastic loss [58]. Near a resonance, the scattering length no longer has a pole, but instead both real and imaginary parts show an oscillation; this may be written as a circle in the complex plane [59],

$$a(B) = a_{\rm bg} + \frac{a_{\rm res}}{2(B - B_{\rm res})/\Gamma_B^{\rm inel} + i}, \tag{7}$$

where $a_{\rm res}$ is a resonant scattering length that characterizes the oscillation. In general, both $a_{\rm bg}$ and $a_{\rm res}$ are complex, but the weak background inelasticity for CsYb means that they are nearly real and we will neglect their complex parts. If $|a_{\rm res}|$ is large, then the oscillation in the real part of the scattering length is large and polelike, similar to the case without decay. $\Gamma_B^{\rm inel}$ is a decay width in field; the decay width in energy is given by $\Gamma_E^{\rm inel} = \Gamma_B^{\rm inel}\delta\mu$, where $\delta\mu$ is the magnetic moment of the bare resonant state relative to the atomic state. When inelasticity is present, the molecule formed by magnetoassociation can decay (predissociate) with lifetime $\tau = \hbar/\Gamma_E^{\rm inel}$. We define the width Δ for a decayed resonance through

$$a_{\rm bg}\Delta = -a_{\rm res}\Gamma_B^{\rm inel}/2. \tag{8}$$

This gives the same behavior in the wings as for an undecayed resonance of the same width [60].

D. Coupled-channel calculations

To locate and characterize the Feshbach resonances, we use coupled-channel bound-state and scattering calculations. The wave function is expanded in an uncoupled basis set

$$|s, m_s\rangle|i_{\rm Cs}, m_{i,{\rm Cs}}\rangle|i_{\rm Yb}, m_{i,{\rm Yb}}\rangle|L, M_L\rangle. \tag{9}$$

Here s, $i_{\rm Cs}$, and $i_{\rm Yb}$ are quantum numbers for the electron and nuclear spin angular momenta and m_s, $m_{i,{\rm Cs}}$, and $m_{i,{\rm Yb}}$ are the corresponding projections onto the axis of the magnetic field. The only conserved quantum numbers are the total angular momentum projection $M_{\rm tot} = m_s + m_{i,{\rm Cs}} + m_{i,{\rm Yb}} + M_L$ and the total parity $(-1)^L$. Basis sets are constructed including all functions of the required $M_{\rm tot}$ and parity $+1$, including functions up to $L_{\rm max}$. Different situations require $L_{\rm max} = 0$, 2, or 4, as described below.

The five bosonic isotopes of Yb all have zero nuclear spin, $i_{\rm Yb} = 0$, and the two fermions, ^{171}Yb and ^{173}Yb, have $i_{171{\rm Yb}} = 1/2$ and $i_{173{\rm Yb}} = 5/2$, respectively. For the Cs atom, $i_{\rm Cs} = 7/2$ and $s = 1/2$; these can be coupled to give a resultant $f = 3$ or 4. The corresponding projection m_f is conserved by $\hat{H}_{\rm Cs}$, but f is not except at $B = 0$. Nonetheless, we label states by the value of f that they correlate with at $B = 0$ [61].

The resulting coupled equations are constructed and solved for bound states using the BOUND and FIELD programs [62,63] and for scattering using the MOLSCAT program [63,64]. In the short-range region, $3.5\,\text{Å} < R < 25$ Å, solutions are propagated using the diabatic log-derivative method of

Manolopoulos [65,66] with a fixed step size 0.001 Å; in the long-range region, 25 Å $\leqslant R \leqslant R_{\rm max}$, the log-derivative Airy propagator of Alexander and Manolopoulos is applied with a variable step size [67]. This allows efficient propagation to very large values of $R_{\rm max}$. The calculations are converged with respect to integration range and step size.

For scattering calculations, log-derivative solutions are propagated outward from short range to a distance $R_{\rm max} =$ 50 000 Å at long range. Since the basis functions (9) are not eigenfunctions of the separated-atom Hamiltonian, the resulting log-derivative matrix at $R_{\rm max}$ is transformed to the separated-atom basis set and then matched to asymptotic boundary conditions to obtain the **K** matrix and then the scattering **S** matrix. The scattering length is obtained as $a(k) = (ik)^{-1}(1 - S_{00})/(1 + S_{00})$, where $k = \sqrt{2\mu E}/\hbar$ is the wave vector and S_{00} is the diagonal S-matrix element in the incoming channel. The kinetic energy in the incoming channel is set to be $E = 100$ nK $k_{\rm B}$, where $k_{\rm B}$ is the Boltzmann constant; this energy is low enough that the resulting scattering length has essentially reached its zero-energy value. We use the algorithms of Frye and Hutson [60] to locate and characterize the Feshbach resonances in the calculated scattering lengths.

For bound-state calculations, one log-derivative solution $\boldsymbol{Y}_{\rm out}(R)$ is propagated outward from short range, and another $\boldsymbol{Y}_{\rm in}(R)$ is propagated inward from $R_{\rm max} = 200$ Å, until both reach a matching point $R_{\rm match} = 6$ Å in the classically allowed region. At a bound-state energy, the matching matrix $\boldsymbol{Y}_{\rm out}(R_{\rm match}) - \boldsymbol{Y}_{\rm in}(R_{\rm match})$ has zero determinant and one of its eigenvalues is zero [68]. BOUND locates eigenenergies by varying the energy of the calculation at fixed magnetic field until the matching condition is met. FIELD operates similarly but varies the magnetic field at fixed energy relative to threshold. This approach allows us to converge efficiently and accurately on bound-state energies and on magnetic fields at which bound states cross threshold. The latter are used as estimates of the positions of Feshbach resonances for characterization by MOLSCAT.

E. Fermi's golden rule

Accurate Feshbach resonance widths can be obtained from coupled-channel scattering calculations, but such calculations do not provide much insight. We therefore use an analysis based on Fermi's golden rule to understand our results. This gives an expression for the resonance width in terms of the matrix element of the coupling operator $\hat{V}_{\rm spin}(R)$ between the single-channel scattering state $|\alpha k\rangle$, which is labeled by a channel index α and wave vector k and normalized to a δ function of energy, and the bound state $|\alpha' n\rangle$, where n is the vibrational quantum number relative to threshold. Brue and Hutson showed that the width can be written [34] as

$$\Delta = \frac{\pi}{k a_{\rm bg} \delta\mu} \langle n|\omega_x(R)|k\rangle_R^2 \langle \alpha'|\hat{\Omega}_x|\alpha\rangle_{\rm spin}^2, \qquad (10)$$

where the matrix element has been separated into a radial component $\langle\cdots\rangle_R$ and a spin component $\langle\cdots\rangle_{\rm spin}$.

The separation of the two components of the matrix element allows a clear interpretation of the factors that influence the resonance widths. The spin component $\langle\alpha'|\hat{\Omega}_x|\alpha\rangle$, which was denoted $I_{m_{f,a}}(B)$ for mechanism I in Ref. [34], describes how the coupling strength depends on the spin states that are coupled and how it varies with magnetic field. The radial component $\langle n|\omega_x(R)|k\rangle$ takes account of the binding energy of the bound state and the background scattering length in the incoming channel. Near threshold, $\langle n|\omega_x(R)|k\rangle$ is proportional to $k^{1/2}$, so that Δ is independent of energy to first order.

The golden rule approach can be used as an approximate method of calculating widths, but in this paper we use it only as an interpretative tool. All widths presented are from coupled-channel calculations.

III. COUPLING MECHANISMS

In this section, we explore the resonances caused by the three principal coupling mechanisms described in Sec. II A. We focus on the general patterns of the resonance positions and widths, rather than the specific predictions, which are given in Sec. IV. We also consider inelastic decay.

We take Cs + ^{173}Yb as our example system in this section, although the analysis is relevant to other isotopologs and other systems formed from an alkali-metal atom and a closed-shell atom, such as Rb + Sr. The scattering length for $V_{\rm elec}(R)$ is very small for Cs + ^{173}Yb, so that $a_{\rm bg}$ can vary substantially between resonances, and it is important to use the normalized width $\bar{\Delta}$ [Eq. (6)] rather than Δ itself as the measure of resonance strength.

A. Mechanism I

Resonances caused by mechanism I have been investigated by Brue and Hutson [34]. However, at that time the binding energies and scattering lengths for Cs + Yb were unknown, so they could study only the general properties.

The operator $\hat{\Omega}_{\rm I} = \hat{i}_{\rm Cs} \cdot \hat{s}$ responsible for mechanism I produces couplings with selection rule $\Delta m_f = 0$, where the notation $\Delta x = x_{\rm bound} - x_{\rm scat}$ indicates the change in quantum number x between the incoming scattering state and the resonant bound state. Since there is only one atomic state of each m_f for each f, mechanism I couples molecular bound states to atomic scattering states only if they have different values of f. Each bound state is essentially parallel to the atomic threshold that supports it, and Fig. 1(b) shows the resulting crossing diagram. The molecular states that produce Feshbach resonances by mechanism I correspond to $f = 4$, so at the energy of the $f = 3$ thresholds they are bound by approximately the Cs hyperfine splitting. The bound states are therefore sparsely distributed in energy and the corresponding resonances are sparsely distributed in magnetic field. The matrix element $\langle f m_f|\hat{\Omega}_{\rm I}|f' m_f\rangle$ goes linearly to zero as $B \to 0$, so the resulting resonance widths $\bar{\Delta}$ are proportional to B^2 at low fields [34]. Resonances with usefully large widths thus exist at accessible magnetic fields only if a bound state for $f = 4$ accidentally falls close to the $f = 3$ thresholds.

Resonances caused by mechanism I are present for both bosonic and fermionic isotopes of Yb. For bosonic isotopes, Yb hyperfine couplings are absent. Since there are no significant anisotropic couplings in this case, we use calculations with $L_{\rm max} = 0$. However, for fermionic isotopes (^{171}Yb and ^{173}Yb) with nonzero nuclear spin, the hyperfine coupling terms corresponding to mechanisms II and III can alter the

resonance widths produced by mechanism I alone and in some cases introduce inelastic decay. These effects are discussed in the following subsections.

B. Mechanism II

Mechanism II is due to the scalar hyperfine coupling between the electron spin and the nuclear spin of a fermionic isotopes of Yb, given by the second term in Eq. (4). We can separate the corresponding operator $\hat{\Omega}_{\rm II} = \hat{i}_{\rm Yb} \cdot \hat{s}$ into three components,

$$\begin{aligned}\hat{\Omega}_{\rm II} &= \hat{\Omega}^0_{\rm II} + \hat{\Omega}^{+1}_{\rm II} + \hat{\Omega}^{-1}_{\rm II} \\ &= \hat{i}_{{\rm Yb},z}\hat{s}_z + \tfrac{1}{2}\hat{i}_{\rm Yb-}\hat{s}_+ + \tfrac{1}{2}\hat{i}_{\rm Yb+}\hat{s}_-,\end{aligned} \tag{11}$$

where $\hat{s}_\pm$ and $\hat{i}_{\rm Yb\pm}$ are raising and lowering operators. The superscripts on the components $\hat{\Omega}^x_{\rm II}$ correspond to the selection rule $\Delta m_f = 0, \pm 1$, and we will similarly refer to mechanisms II^0, II^{+1}, and II^{-1}. These calculations use $L_{\rm max} = 2$ in order to take account of inelastic decay as discussed in Sec. III D.

The selection rule on Δm_f is less restrictive for mechanism II than for mechanism I and allows Feshbach resonances with $\Delta f = 0$ as well as $\Delta f = 1$. Figure 2 shows how the bound states cross the $f = 3$ and $f = 4$ scattering thresholds for Cs + ^{173}Yb. We consider resonances that arise at crossings where there are direct couplings due to mechanism II, which are shown as circles, squares, and triangles for mechanisms II^0, II^{+1}, and II^{-1}, respectively.

Many more resonances arise than for mechanism I. In particular, there is a set of resonances at low field, where the thresholds are crossed by the least-bound state ($n = -1$) with the same f but $\Delta m_f = -1$ for $f = 3$ or $\Delta m_f = +1$ for $f = 4$. The corresponding resonance positions are approximately

$$B_{\rm res}(n = -1) = \frac{(2i_{\rm Cs} + 1)}{|\Delta m_f| g_s \mu_{\rm B}} E_{\rm b}(n = -1), \tag{12}$$

where $E_{\rm b}(n = -1)$ is the binding energy of the least-bound state at $B = 0$. For Cs + ^{173}Yb, Eq. (12) gives $B_{\rm res}(n = -1) = 163$ G, consistent with the crossings shown in Fig. 2. The deviations from Eq. (12) are at most a few G and arise principally from the nonlinearity of the atomic Zeeman effect. The resonance position from the least-bound state with $\Delta f = 0$ is approximately the same in the $f = 3$ and $f = 4$ manifolds. Even for a system where the binding energy is unknown, the least-bound state is always within $36\hbar^2/(2\mu\bar{a}^2)$ of threshold [69], and resonances of this type exist provided f remains a nearly good quantum number at fields up to $B_{\rm res}(n = -1)$; this is the case for Cs or Rb interacting with either Yb or Sr.

There are also resonances where bound states with $n = -2$ cross thresholds with the same f. These start around $B = 1200$ G, but are much more spread out in field than those for $n = -1$ because the atomic Zeeman effect is nonlinear at higher fields.

Each crossing point in Fig. 2 gives rise to a set of closely spaced resonances due to states with different $m_{i,\rm Yb}$, as shown schematically in Fig. 3. Resonances for different $m_{i,\rm Yb}$ have different widths, as discussed below. The selection rule on the nuclear spin projection is $\Delta m_{i,\rm Yb} = -\Delta m_f$; thus Feshbach resonances occur at different crossing points in the pattern for mechanisms II^0, II^{+1}, and II^{-1}, indicated by circles, squares, and triangles respectively. The splitting of the threshold levels is determined solely by the Yb nuclear Zeeman term in Eq. (3), while the splitting of the molecular levels has an additional contribution from the diagonal matrix elements associated with mechanism II. Without this additional contribution, all the resonances for the same value of Δm_f would occur at the same field, but its presence separates the resonances for different $m_{i,\rm Yb}$.

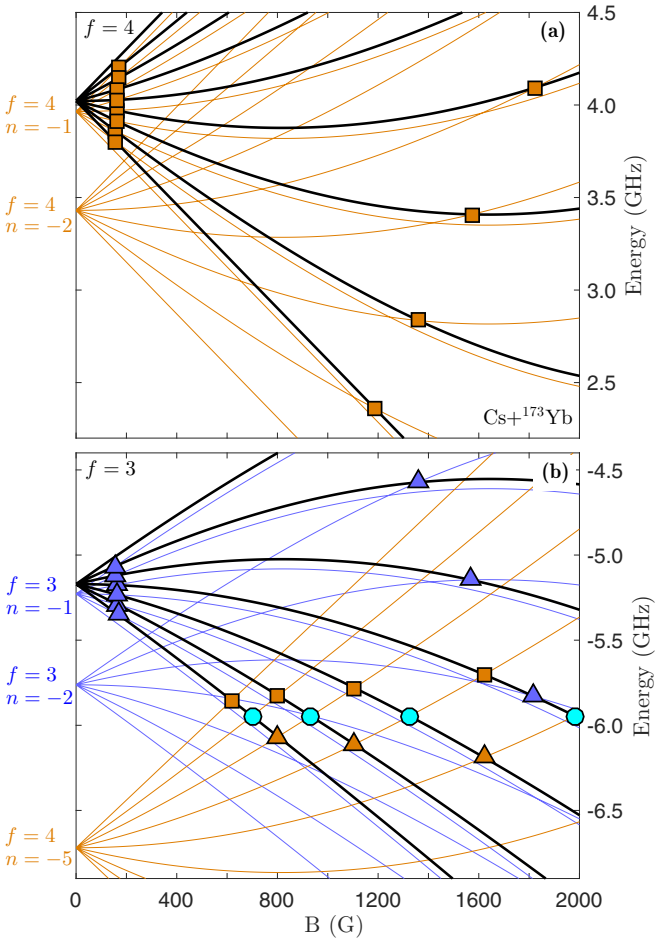

FIG. 2. Level-crossing diagram with Feshbach resonance positions from mechanism II for Cs +^{173}Yb. The atomic thresholds (thick black lines) are from the upper ($f = 4$) and lower ($f = 3$) hyperfine manifolds in panels (a) and (b), respectively. The quantum numbers f and n are given on the left-hand side for each manifold of molecular levels (thin colored lines). The solid squares, circles, and triangles show the positions of Feshbach resonances caused by mechanism II, with $\Delta m_f = +1$, 0, and -1, respectively.

General properties of the widths of the resonances can be inferred from Fermi's golden rule. By contrast with mechanism I, the spin factor in the resonance widths, $\langle\alpha'|\hat{\Omega}_{\rm II}|\alpha\rangle^2$, does not fall to zero as $B \to 0$. This might seem to suggest usefully large widths for the $\Delta f = 0$ resonances that are guaranteed to exist at low field. However, the radial contribution to the resonance widths, $\langle n|\omega_{\rm II}(R)|k\rangle^2$, is proportional to $E_{\rm b}^{2/3}$ [34], where $E_{\rm b}$ is the binding energy of the resonant state below the threshold that supports it; through Eq. (12), the width is thus proportional to $B_{\rm res}^{2/3}$. Thus, although low-field $\Delta f = 0$ resonances arising from mechanism II are guaranteed

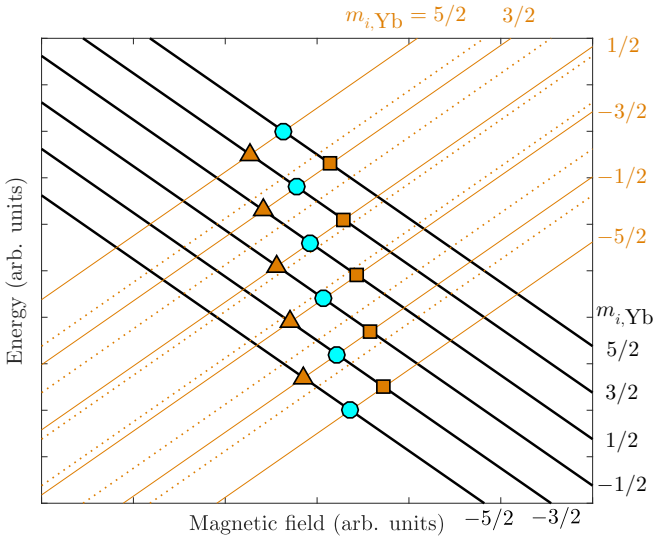

FIG. 3. Schematic diagram demonstrating the splitting pattern for a set of resonances arising from a single crossing in Fig. 2, caused by mechanism II for Cs + ^{173}Yb. The atomic thresholds (thick black lines) and molecular bound states (thin brown lines) are labeled by $m_{i,\mathrm{Yb}}$. The solid squares, circles, and triangles indicate the resonance positions for sets with $\Delta m_f = +1$, 0, and -1, respectively; only one set appears at each crossing in Fig. 2. The dotted lines show the bound states without shifts due to mechanism II. The energy spacings are typically less than 1 MHz and the set of resonances typically spans less than 1 G.

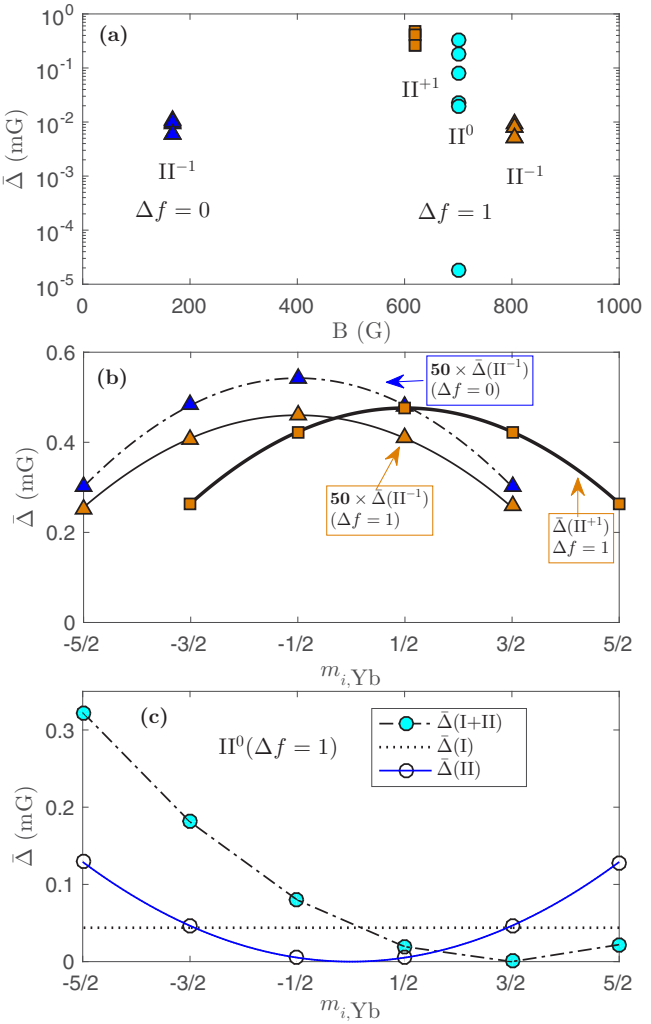

FIG. 4. Widths of the resonances caused by mechanism II for Cs + ^{173}Yb. Symbols correspond to those in Fig. 2. (a) Overview of the sets of resonances arising from the four crossings at the $f = 3$, $m_f = 3$ threshold in Fig. 2. (b) Widths within each set with $\Delta m_f = \pm 1$ as a function of $m_{i,\mathrm{Yb}}$. The lines connecting the points are parabolas as expected from Fermi's golden rule. (c) Widths within the set with $\Delta m_f = 0$, showing separate contributions from mechanisms I and II and their combination.

to exist, their widths are also somewhat suppressed, albeit more weakly and for different reasons than for those arising from mechanism I.

There are also $\Delta f = 1$ resonances from mechanism II at the $f = 3$ thresholds. At each threshold, these occur in three sets, corresponding to the three allowed values of Δm_f. As for the resonances arising from mechanism I, which also have $\Delta f = 1$, these resonances exist at low fields only if the binding energies are favorable. As shown in Fig. 2, they exist for ^{173}Yb at the lowest ($m_f = 3$) threshold at fields from about 600 G upward and from progressively higher fields at excited thresholds.

The four sets of resonances at the $m_f = 3$ thresholds are examined in Fig. 4; three sets have $\Delta f = 1$ and one has $\Delta f = 0$. The normalized resonance widths are shown as a function of their resonance positions in Fig. 4(a) and as a function of $m_{i,\mathrm{Yb}}$ in Figs. 4(b) and 4(c). For the $\mathrm{II}^{\pm 1}$ resonances shown in Fig. 4(b), the resonance widths are proportional to $[i_{\mathrm{Yb}}(i_{\mathrm{Yb}} + 1) - m_{i,\mathrm{Yb}}(m_{i,\mathrm{Yb}} \mp 1)]$; this arises simply from the factors due to the lowering and raising operators $\hat{i}_{\mathrm{Yb}\mp}$ in $\hat{\Omega}^{\pm 1}$ [33]. For the II^{0} resonances, the pattern of widths is more complicated because the atomic scattering and molecular bound states are coupled by both mechanisms I and II. The resonance widths as a function of $m_{i,\mathrm{Yb}}$ are shown in Fig. 4(c) for each mechanism separately and for the combination. For mechanism I alone, the Yb nuclear spin is not involved, so the width is constant at $\bar{\Delta} = 0.04$ mG. For mechanism II alone, the width is proportional to $m_{i,\mathrm{Yb}}^2$ due to the operator $\hat{i}_{\mathrm{Yb},z}$ in $\hat{\Omega}^0_{\mathrm{II}}$. However, the actual resonance width $\bar{\Delta}(\mathrm{I} + \mathrm{II})$ is proportional to the square of the sum of the coupling matrix elements. This increases the widths for negative $m_{i,\mathrm{Yb}}$ and reduces those for positive $m_{i,\mathrm{Yb}}$.

The relative strengths of different sets depend strongly on the electron-spin components of the states that are coupled. For example, for the II^{-1} set near 200 G, the spin-dependent matrix element $\langle \alpha' | \hat{i}_{\mathrm{Yb}} \cdot \hat{s} | \alpha \rangle$ is shown as a function of magnetic field in Fig. 5(a). For this resonance, the dominant electron-spin component is $|m_s = -1/2\rangle$ in both the scattering and bound states, but the resonance coupling is actually between $|m_s = 1/2\rangle_{\mathrm{scat}}$ and $|m_s = -1/2\rangle_{\mathrm{bound}}$. The small proportion of $m_s = 1/2$ in the scattering state limits the coupling and so the final resonance width. This component vanishes at high field, so the matrix elements $\langle \alpha' | \hat{i}_{\mathrm{Yb}} \cdot \hat{s} | \alpha \rangle$ in Fig. 5(b) approach zero.

A similar argument applies to the sets of resonances with $\Delta f = 1$ and $\Delta m_f = \pm 1$. The corresponding spin-dependent

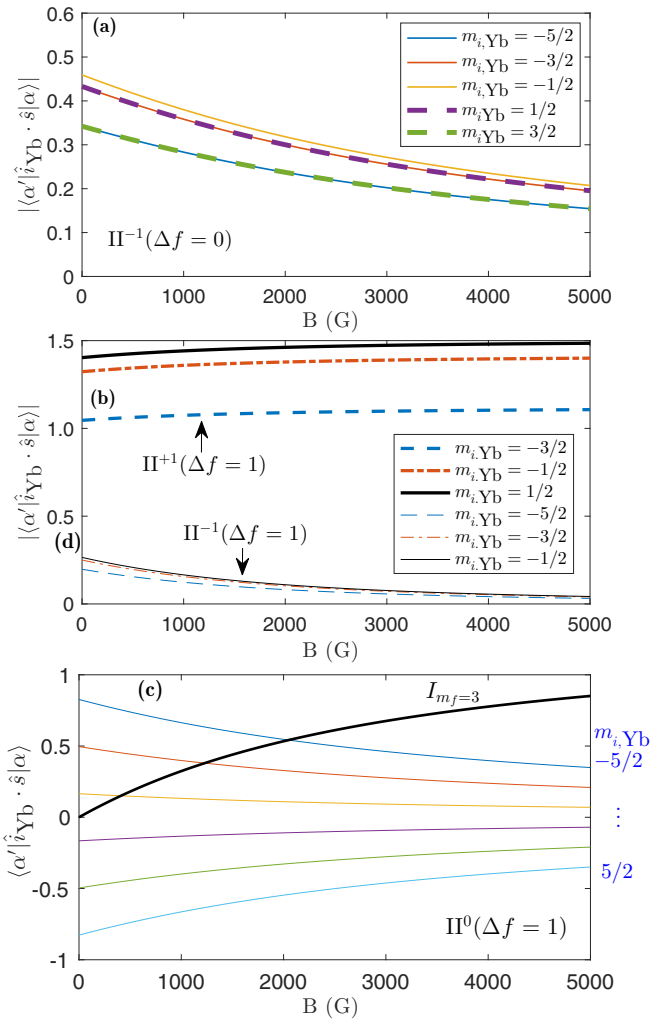

FIG. 5. Spin components $\langle\alpha'|\hat{i}_{\mathrm{Yb}}\cdot\hat{s}|\alpha\rangle$ of coupling matrix elements for mechanism II. (a) Absolute values of matrix elements for resonances due to bound states with $f = 3$, $m_f = 2$ at the $f = 3$, $m_f = 3$ threshold, as a function of field, for different $m_{i,\mathrm{Yb}}$. (b) Absolute values of matrix elements for resonances due to bound states with $f = 4$, $m_f = 2$ or 4 at the $f = 3$, $m_f = 3$ threshold. (c) Matrix elements for resonances due to bound states with $f = 4$, $m_f = 3$ at the $f = 3$, $m_f = 3$ threshold. The matrix element for mechanism I is shown as a thick black line; it adds constructively for $m_{i,\mathrm{Yb}} < 0$ and destructively for $m_{i,\mathrm{Yb}} > 0$.

matrix elements are shown in Fig. 5(b). For both these sets, the dominant electron-spin component is $|m_s = 1/2\rangle$ in the scattering state and $|m_s = -1/2\rangle$ in the bound state. Mechanism II^{+1} couples these two dominant spin components, but II^{-1} couples the smaller components that vanish at high field. Consequently, the II^{+1} resonances have much larger widths than the II^{-1} resonances, as shown in Fig. 4(b).

C. Mechanism III

Mechanism III is due to the tensor, or anisotropic, hyperfine coupling on the Yb nucleus, described by the third term in Eq. (4). Like mechanism II, it exists only for the fermionic isotopes of Yb. Unlike mechanisms I and II, this anisotropic coupling can change the rotation of the molecule, with selection rule $\Delta L = 2$; there are also $\Delta L = 0$ terms

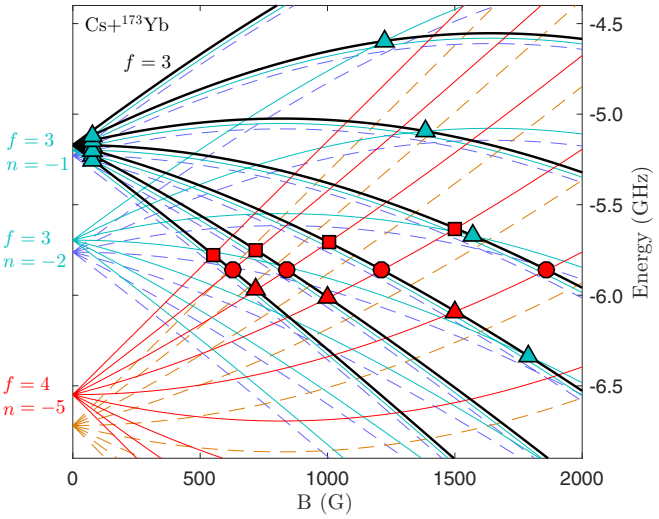

FIG. 6. Level-crossing diagram with Feshbach resonances from mechanism III for Cs $+^{173}$Yb. The threshold levels shown (heavy black lines) are from the lower hyperfine manifold with $f = 3$. The quantum numbers f and n are labeled on the left-hand side for each manifold of molecular levels (thin colored lines with solid lines for $L = 2$ and dashed lines for $L = 0$). The solid squares, circles, and triangles indicate the positions of Feshbach resonance caused by mechanism III, with $\Delta m_f = +1$, 0, and -1, respectively.

due to this term, but not for $L = 0$. Resonances in s-wave scattering arising from direct coupling due to mechanism III must therefore come from bound states with $L = 2$. The other selection rules are $\Delta m_f = 0, \pm 1$ and $\Delta m_{i,\mathrm{Yb}} = 0, \pm 1$. By contrast with mechanism II, a change in $\Delta m_f + \Delta m_{i,\mathrm{Yb}}$ may be compensated by $\Delta M_L \neq 0$ to conserve M_{tot}. The explicit form of the spin-coupling operator $\hat{\Omega}_{\mathrm{III}}$ is more complicated than for mechanism II, but it can still be separated by analogy with Eq. (11) into terms proportional to $\hat{s}_z$, $\hat{s}_+$, and $\hat{s}_-$. We thus subdivide mechanism III into mechanisms III^0, III^{+1}, and III^{-1}, respectively. These calculations use $L_{\max} = 4$ in order to take account of inelastic decay as discussed in Sec. III D.

Figure 6 shows the $L = 2$ bound states and the resulting Feshbach resonances arising from direct coupling due to mechanism III at the $f = 3$ thresholds for Cs $+^{173}$Yb. The $L = 0$ bound states are shown as dashed lines for comparison and are identical to those in Fig. 2(b). Each $L = 2$ state is immediately above the associated $L = 0$ state, with a spacing proportional to an effective rotational constant, which varies strongly with the binding energy of the state [70]. This produces a pattern of resonances very similar to that for mechanism II, but shifted to somewhat lower field and with additional splittings. Because of the similar separation of the operator into terms proportional to $\hat{s}_z$, $\hat{s}_+$, and $\hat{s}_-$, the general conclusions about resonance widths for mechanism II hold for mechanism III as well.

The most significant difference between mechanisms II and III is in the internal structure of the sets of resonances. Since the bound states for mechanism III have $L = 2$, there are five times as many states, corresponding to different values of M_L. Because of the larger number of states, more individual crossings within a set can cause Feshbach resonances, and there can be multiple resonances at each threshold. Within the

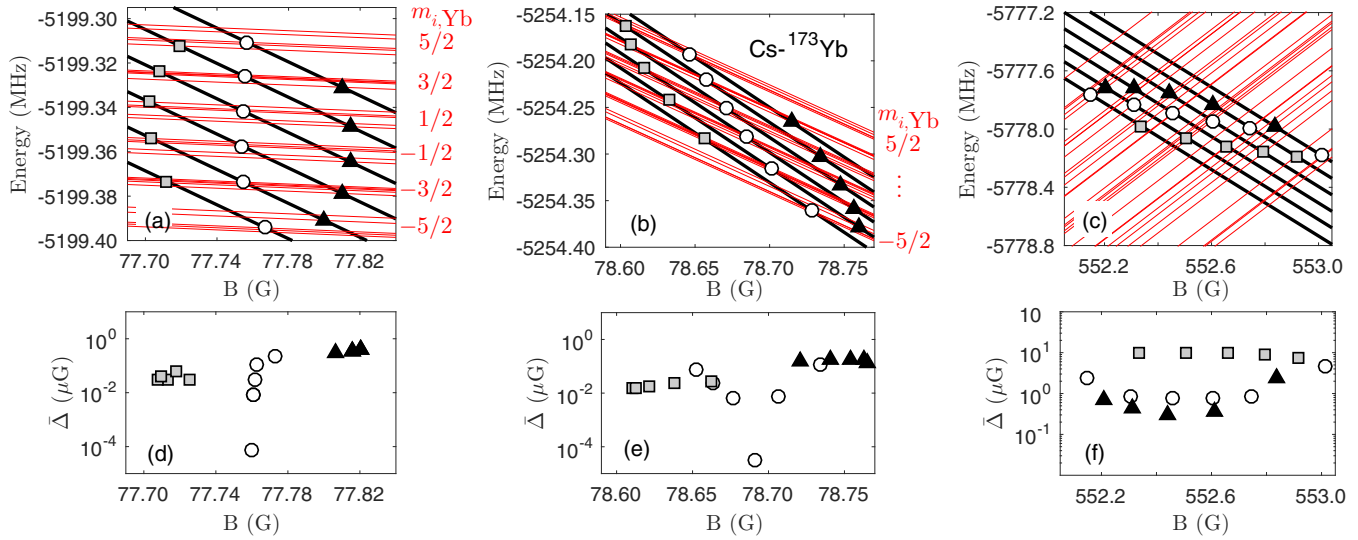

FIG. 7. Structure of sets of resonances caused by mechanism III for Cs + ^{173}Yb. Panels (a), (b), and (c) show bound-state levels (thin red lines) crossing thresholds (thick black lines) for three representative resonances, with crossings that cause Feshbach resonances due to direct couplings marked by symbols. Grey squares, white circles, and black triangles show resonances with $\Delta m_{i,\mathrm{Yb}} = +1$, 0, and -1, respectively. Panels (d), (e), and (f) show the corresponding normalized resonance widths $\bar{\Delta}$ as a function of magnetic field. [(a), (d)] Set of resonances near 78 G at the ($f = 3$, $m_f = 1$) threshold; [(b), (e)] set of resonances near 79 G at the ($f = 3$, $m_f = 3$) threshold; and [(c), (f)] set of resonances near 552 G at the ($f = 3$, $m_f = 3$) threshold.

set of bound states for each M_{tot}, the states with different M_L and $m_{i,\mathrm{Yb}}$ are mixed by coupling due to mechanism III and the Yb quadrupole term. There are additional small effects due to spin-rotation and Cs quadrupole coupling. However, the nuclear Zeeman effect and the diagonal matrix elements due to mechanism II separate the states according to $m_{i,\mathrm{Yb}}$, and these splittings are generally larger than the couplings between them; accordingly, $m_{i,\mathrm{Yb}}$ and M_L remain useful labels, even though they are not fully conserved.

Figure 7 shows the crossing diagrams and the widths of the resonances in each set as a function of position for three typical examples. The first example is the set of resonances due to bound states with $f = 3$, $m_f = 0$, and $n = -1$ crossing the $f = 3$, $m_f = 1$ threshold. In this case, the splitting between the bound states is similar to that between the thresholds. This is because the diagonal matrix elements of mechanisms II and III are both proportional to the expectation value $\langle m_s \rangle$ of the electron spin projection, and the bound states have $m_f = 0$, for which $\langle m_s \rangle = 0$ at low field. However, states with the same $m_{i,\mathrm{Yb}}$ but different M_L are separated by the Yb quadrupole term. The resulting resonances are separated into three subsets corresponding to $\Delta m_{i,\mathrm{Yb}} = +1, 0, -1$, shown in Fig. 7 by gray squares, open circles, and black triangles, respectively. The splitting between the subsets is governed mostly by the nuclear Zeeman effect and is approximately $g_{\mathrm{Yb}}\mu_{\mathrm{B}}B/\Delta\mu$. The patterns of widths for different $m_{i,\mathrm{Yb}}$ within these subsets resemble those seen in Figs. 4(b) and 4(c) for mechanism II but are distorted by the mixing of the states.

The second example is a similar set of resonances with $\Delta f = 0$, but due to $f = 3$, $m_f = 2$ bound states crossing the $f = 3$, $m_f = 3$ threshold. In this case, the expectation value $\langle m_s \rangle$ for the bound states is not near zero, so the molecular states have substantially different splittings to the thresholds. This separates each of the three subsets (corresponding to $\Delta m_{i,\mathrm{Yb}} = +1, 0, -1$) according to $m_{i,\mathrm{Yb}}$, such that the subsets just overlap in field. The widths are shown in Fig. 7 and again show the expected patterns with respect to $m_{i,\mathrm{Yb}}$. However, the resonances near the middle of this pattern are the narrowest, so that in loss spectroscopy the resonances would effectively form *two* groups in field.

The third example is also at the $m_f = 3$ threshold, but from a set of resonances with $\Delta f = 1$. The $f = 4$ bound states that cause these resonances are more deeply bound, so the diagonal matrix elements of the spin-dependent terms are much larger. The bound states can still be labeled by $m_{i,\mathrm{Yb}}$, but the effect of mechanism II is so large that the ordering of the bound states is reversed from that of the thresholds. The splittings between states with the same $m_{i,\mathrm{Yb}}$ but different M_L, due to mechanism III and the Yb quadrupole term, are also much larger, such that the multiplets overlap in some cases. The three subsets with different values of $\Delta m_{i,\mathrm{Yb}}$ now completely overlap. As a result, there is no obvious structure in the pattern of widths as a function of field.

These three examples qualitatively explain the patterns observed in loss spectroscopy of similar resonances in ^{87}Rb + ^{87}Sr [41]. Figure 1 of Ref. [41] showed loss patterns for three different sets of resonances due to mechanism III. One of these was for a set of resonances due to bound states with $f = 1$, $m_f = 0$ crossing the $f = 1$, $m_f = 1$ threshold; these bound states have $\langle m_s \rangle \sim 0$ and so produce a triple peak as in example 1 above. Another was for a set of resonances due to bound states with $f = 1$, $m_f = -1$ crossing the $f = 1$, $m_f = 0$ threshold; these bound states have $\langle m_s \rangle \neq 0$, and so produce a double peak as in example 2 above. The third was for a set of resonances due to bound states with $f = 2$, $m_f = -2$ crossing the $f = 1$, $m_f = -1$ threshold; these deeper

bound states are more strongly split and mixed with one another, and so produce an unresolved peak as in example 3 above.

D. Inelastic decay

Feshbach resonances show signatures of decay when the bound state couples to inelastic (open) channels below the incoming channel. The primary quantity used to characterize decay in our calculations is the inelastic decay width $\Gamma_B^{\rm inel}$. However, the effect of decay on experiments is better quantified by the lifetime τ and the resonant scattering length $a_{\rm res}$. If the magnitude of $a_{\rm res}$ is too small, the oscillation in the scattering length may not be sufficient to produce measurable loss in two-body or three-body loss spectroscopy; at least $a_{\rm res} > 100\ a_0$ is probably necessary to produce measurable loss rates. If the lifetime is too short, molecules formed by magnetoassociation at the resonance will predissociate before further experimental steps; this may pose a problem if the lifetimes are milliseconds or less.

For the bosonic isotopes of Yb, mechanism I couples the resonant bound state only to the incoming channel. For collisions at magnetically excited Cs thresholds, the Cs quadrupole and tensor hyperfine couplings can in principle cause decay to inelastic channels with $L = 2$, but these terms are small and the associated decay is very weak. For example, for the resonance near 654 G for Cs ($f = 3$, $m_f = -3$) interacting with ^{168}Yb, we calculate $a_{\rm res} = 3.0 \times 10^{10}\ a_0$, corresponding to $\tau = 2.2 \times 10^5$ s. In the remainder of this paper, we carry out calculations on bosonic isotopes using $L_{\rm max} = 0$, which suppresses this weak decay.

For the fermionic isotopes of Yb, any of the coupling operators in Eq. (4) may cause decay, depending on the character of the resonance. However, there are two situations where there is guaranteed to be very little decay. The first is for resonances at the lowest Cs hyperfine threshold ($f = 3$, $m_f = 3$). These can in principle decay to $L = 2$ channels with different $m_{i,\rm Yb}$, but the associated kinetic energy release is very small and inelasticity is strongly suppressed by centrifugal barriers in the outgoing channels. The second is for $\rm II^{-1}$ resonances at $f = 3$ thresholds. For these, the inelastic channels have $\Delta m_f \geqslant 1$ relative to the incoming channel, and thus $\Delta m_f \geqslant 2$ relative to the bound state. There is no direct coupling from such bound states to inelastic channels.

For the remaining resonances in fermionic systems, direct decay pathways exist. Resonances at thresholds with $f = 4$ can always decay to $f = 3$. This results in significant decay, with $a_{\rm res}$ in the range 19 to 125 a_0 for the resonances due to $n = -1$ states, corresponding to $\Gamma_B^{\rm inel}$ from -40 to -120 μG and lifetimes from 3.7 to 10 ms. At $f = 3$, $m_f < 3$ thresholds, resonances due to mechanisms I and $\rm II^0$ can decay by mechanisms $\rm II^{+1}$ and $\rm III^{+1}$, while those due to mechanism $\rm II^{+1}$ can also decay by mechanisms I, $\rm II^0$, and $\rm III^0$. The resulting decay widths and lifetimes show considerable variation with $m_{i,\rm Yb}$ but are generally comparable to those at $f = 4$ thresholds; however, $a_{\rm res}$ is considerably larger because $\bar{\Delta}$ is larger.

For resonances due to mechanism III, the general patterns of decay are similar to those for resonances due to mechanism II. There are additional decay pathways to open channels with $L = 4$, which sometimes contribute up to 80% of the decay widths.

IV. PROMISING RESONANCES FOR EXPERIMENTAL STUDY

In this section, we make specific predictions for Feshbach resonances that appear promising for experimental investigation. We consider resonances in collisions involving Cs in both its ground state ($f = 3$, $m_f = 3$) and magnetically excited states. We highlight the most promising resonances for each Yb isotope at magnetic fields below 2000 G. Tabulations of $B_{\rm res}$, $\bar{\Delta}$, Δ, $a_{\rm bg}$, and where appropriate $a_{\rm res}$, $\Gamma_B^{\rm inel}$, and τ are given in the Supplemental Material [44] for all resonances at magnetic fields up to 5000 G.

There are two experimental situations of particular interest. The first is observation of resonances through their enhancement of collisional processes such as three-body recombination, two-body inelastic loss, or interspecies thermalization; this is commonly known as Feshbach spectroscopy. The second is magnetoassociation of pairs of atoms to form weakly bound molecules, which may be carried out either in an optical trap or in the cells of an optical lattice.

A. Intraspecies Cs collisions

Any experiment carried out in an optical trap is subject to losses due to intraspecies as well as interspecies collisions. Even in its ground state ($f = 3$, $m_f = 3$), ultracold Cs suffers from strong three-body losses at most magnetic fields, due to large intraspecies scattering lengths. Similar losses exist in magnetically and hyperfine excited states, supplemented by two-body inelastic losses. The scattering length $a(B)$ was tabulated for the ground state by Berninger *et al.* [71]. We have recently carried out scattering calculations for pairs of excited Cs atoms in the same state (f, m_f), using the interaction potentials of Ref. [71], for all $f = 3$ and $f = 4$ states [72]. We tabulated both the complex scattering length $a_{\rm Cs} = \alpha_{\rm Cs} - i\beta_{\rm Cs}$ and the rate coefficient $k_{2,\rm Cs}$ for intraspecies two-body loss. We estimate that values of $k_{2,\rm Cs}$ higher than about 10^{-12} cm^3 s^{-1} will obscure losses due to interspecies Feshbach resonances.

For experiments in an optical trap, we estimate that intraspecies scattering lengths larger than about 2000 a_0 will produce three-body losses dominated by intraspecies collisions. Even for scattering lengths at the upper end of this range, it will probably be necessary to work with Cs densities below 10^{12} cm^{-3} to moderate intraspecies three-body losses and with Yb atoms in large excess so that Cs losses due to resonant interspecies collisions are competitive.

For each interspecies resonance in the tables below, and in the Supplemental Material [44], we give calculated values of $\alpha_{\rm Cs}$ and $k_{2,\rm Cs}$, where it exists, at the resonance position.

B. Experimental considerations

1. Experiments in optical traps

Optical traps may be used to trap atoms in any internal state and allow independent control of the applied magnetic field. Although the atomic cloud is confined to a small volume,

there is nevertheless always some variation in the magnetic field across the sample. This may arise from a magnetic field gradient used to levitate the atoms or from other sources such as curvature in the bias field. There is also inevitably some time variation of the field, typically on the order of a few mG. For the narrow resonances predicted in Cs + Yb, it is likely that only a part of the cloud will be on resonance at any one time. The resulting loss signal will then be proportional to the range of fields over which $|a(B)|$ exceeds a critical value $a_{\rm crit}$. For resonances in elastic scattering, this range is proportional to $a_{\rm bg}\Delta$. As described above, for Cs + Yb we have chosen to tabulate the normalized width $\bar{\Delta} = (a_{\rm bg}/\bar{a})\Delta$, which retains the dimensions of field. The narrowest resonance observed in recent experiments on RbSr [41] had a calculated normalized width $\bar{\Delta} = 0.0043$ mG. In this section, we tabulate resonances for which $\bar{\Delta} > 0.04$ mG, except below 200 G, where we tabulate resonances with $\bar{\Delta} > 0.004$ mG.

Feshbach resonances may also be detected through enhanced interspecies thermalization [73]. This is particularly attractive for Cs + ^{173}Yb, where the background scattering length is very low and there will be very little interspecies thermalization away from resonance. The rate of interspecies thermalization is also expected to be approximately proportional to $\bar{\Delta}$.

Cs atoms in $f = 4$ excited states are predicted to decay quickly by two-body inelastic processes [72]. We therefore focus on Cs + Yb resonances involving Cs atoms in $f = 3$ states. For bosonic isotopes of Yb at any threshold and for fermionic isotopes at the lowest threshold, the interspecies resonances are undecayed and the scattering length passes through a pole at resonance. However, for fermionic isotopes at thresholds with $m_f < 3$, the resonances may be decayed, as described in Sec. III D; the pole is then replaced by a more complicated line shape, which for the resonances considered here is an essentially symmetric oscillation of amplitude $\pm a_{\rm res}/2$. If $a_{\rm res}$ is less than about 100 a_0, an interspecies resonance may not produce a significant peak in three-body loss.

Interspecies two-body loss occurs only with fermionic isotopes of Yb in combination with excited states of Cs. It is very weak away from resonance but shows a narrow peak of height proportional to $a_{\rm res}$ at resonance. There may be some resonances and conditions under which interspecies two-body loss is faster than three-body loss.

2. Experiments in lattices

Experiments in three-dimensional (3D) optical lattices have several advantages. By loading quantum-degenerate gases into the lattice and exploiting the superfluid-to-Mott-insulator transition [74], the number of atoms loaded onto a lattice site can be controlled and tunneling suppressed. Under such conditions, intraspecies losses can be completely eliminated. Experiments may thus be performed with any internal state and at any magnetic field, without restriction on the intraspecies scattering properties; this is particularly beneficial when working with atoms such as Cs, where intraspecies loss may otherwise be a limiting factor. The use of an optical lattice also removes the need for a field gradient to levitate the cloud against gravity.

Experiments in lattices are still subject to interspecies two-body loss when it is present. For fermionic isotopes of Yb, combined with excited states of Cs, it may be possible to detect resonances by searching for two-body loss as a function of magnetic field in a lattice.

3. Magnetoassociation

Magnetoassociation may be carried out either in an optical trap or in a lattice cell containing one atom of each type. In a confined system, the scattering continuum above threshold is replaced by a series of quantized translational levels. A scattering resonance then appears as a series of avoided crossings between the molecular states and these quantized levels. The strengths (energy widths) of the avoided crossings are proportional to $(a_{\rm bg}\Delta)^{1/2}$ [55,56]. In magnetoassociation, the goal is to sweep the magnetic field across the lowest of the avoided crossings slowly enough to achieve adiabatic passage. The maximum sweep speed that achieves this is proportional to the square of the strength and thus to $a_{\rm bg}\Delta$ [55,56]. Because of this, $\bar{\Delta}$ is an appropriate measure of the resonance width for magnetoassociation as well as for loss spectroscopy.

A lattice cell confines a pair of atoms more tightly than an optical trap, increasing the strength of the avoided crossing available for magnetoassociation. The strength is proportional to $\omega^{3/4}$ [55,56], where ω is the harmonic trap frequency [75]. The maximum speed of the field sweep is thus proportional to $\omega^{3/2}$.

For a broad resonance, it is relatively easy to sweep the field slowly enough to achieve adiabatic passage. However, for narrow resonances such as those considered here, it is more challenging. Field inhomogeneity results only in different parts of the sample crossing the resonance at different times. Field noise, however, may result in repeated crossing and recrossing at speeds that cause nonadiabatic transitions and loss. Very narrow resonances thus require very stable fields.

4. Molecular lifetimes

Molecules formed by magnetoassociation at a decayed resonance may themselves decay (predissociate) spontaneously with lifetime τ, as described in Sec. II C. In practical terms, it is necessary to stabilize the magnetic field after the magnetoassociation sweep, before transferring the molecules to another state. This is likely to be difficult if the molecular lifetime is less than about 100 μs.

C. Cs + bosonic Yb

For Cs interacting with bosonic isotopes of Yb, there are only a few resonances located below 2000 G. These are all caused by mechanism I. Inelastic decay is negligible for these resonances, even for excited states of Cs, as discussed in Sec. III D. The important properties are the resonance position and width, as well as the properties relevant to background loss of Cs for experiments in an optical trap. Table III lists all resonances that meet the width criteria described above, together with some additional ones that warrant discussion.

The resonances for ^{176}Yb are the strongest in Table III and also have small two-body loss rates for Cs. The pair of

TABLE III. Experimentally promising resonances in ultracold collisions between Cs and bosonic isotopes of Yb.

Cs-Yb	m_f	$B_{\rm res}$ (G)	$\bar{\Delta}$ (mG)	$\alpha_{\rm Cs}$ (a_0)	$k_{2,\rm Cs}$ (cm^3 s^{-1})
133–168	−3	654	−0.074	1.59×10^3	2.25×10^{-13}
133–170	−1	366	−0.098	3.53×10^3	2.41×10^{-11}
	−1	1273	1.2	1.99×10^2	9.62×10^{-11}
133–172	2	602	0.051	1.91×10^3	1.75×10^{-11}
	1	914	0.19	-1.89×10^5	9.70×10^{-12}
	0	1528	0.64	7.10×10^2	1.76×10^{-13}
133–174	3	964	0.17	1.11×10^3	
	2	1252	0.60	1.21×10^3	2.91×10^{-14}
	1	1699	1.6	1.26×10^3	2.15×10^{-13}
133–176	3	1497	5.9	2.43×10^3	
	2	1866	18	2.20×10^3	1.33×10^{-13}
	−3	1559	−35	1.16×10^3	1.22×10^{-13}
	−3	3359	160	2.31×10^2	4.79×10^{-14}

resonances near 1559 and 3359 G are from a double crossing between the atomic and molecular states with $m_f = -3$. The relatively large normalized widths $\bar{\Delta}$ for these occur both because the background scattering length is large (798 a_0) and because the difference between the magnetic moments of the atomic and molecular states is small near such a double crossing [34]. The resonance at 3359 G is included in Table III, despite its high field, because it is unusually wide and is also in a field range where three-body loss of Cs is expected to be relatively slow. These resonances are promising for loss spectroscopy. However, ^{176}Yb has a small negative intraspecies scattering length [76], which leads to collapse of its condensates [77], so that a lattice with a high filling fraction will be hard to produce.

The Yb isotopes that are most easily cooled to degeneracy, and are thus most suitable for formation of Mott insulators, are ^{174}Yb [78] and ^{170}Yb [79]. The normalized widths of the resonances for these isotopes are smaller than for ^{176}Yb, but magnetoassociation in an optical lattice may still be feasible. For ^{170}Yb, two-body loss of Cs atoms may prevent observation of the resonances by loss spectroscopy. The three resonances for ^{174}Yb appear more suitable for loss spectroscopy, though three-body losses of Cs atoms are expected to be fairly fast.

^{172}Yb has a large negative intraspecies scattering length [76] and has not been cooled to degeneracy. It nevertheless has resonances that may be observable by loss spectroscopy. The resonance near 1528 G for ^{172}Yb with Cs ($f = 3$, $m_f = 0$) appears particularly suitable for this because of the relatively small background losses expected for Cs atoms.

^{168}Yb has a very low isotopic abundance and the only resonance available below 2000 G is the one near 654 G. This resonance might be observable by loss spectroscopy but has no obvious advantages over those for more abundant isotopes.

D. Cs + fermionic Yb

For Cs interacting with fermionic isotopes of Yb, resonances can be driven by any of the three mechanisms discussed in Sec. III. This provides more resonances than for bosonic isotopes, particularly at low field. The resonances that meet the criteria described above are listed in Table IV for ^{171}Yb and Table V for ^{173}Yb. Each entry in the tables represents a set of closely spaced resonances corresponding to different values of $m_{i,\rm Yb}$ (and M_L for mechanism III), as described in Sec. III. For each set, only the widest is given. Full tabulations of the resonances, including all those in each set and those that are excluded from Tables IV and V by one or more of the criteria, are given in the Supplemental Material [44].

The resonances for ^{171}Yb follow similar patterns to those for ^{173}Yb, discussed in Sec. III. For ^{171}Yb, there is a group of resonances around 74 G caused by bound states with $n = -1$ crossing thresholds with the same value of f. These are all caused by mechanism II. The corresponding resonances from $n = -2$ states start around 900 G. The remaining resonances arise from bound states with $f = 4$ crossing $f = 3$ thresholds and arise from mechanisms I and II. The $n = -5$ bound state with $f = 4$ lies approximately 360 MHz below the $f = 3$ threshold at zero field; it causes resonances starting around 150 G. At each threshold, there are resonances of this type with $\Delta m_f = +1, 0$, and -1, at progressively increasing fields, though not all of them meet the criteria for inclusion in Table IV.

Most of the resonances for fermionic Yb are subject to decay. Tables IV and V include values of the resonant scattering length $a_{\rm res}$ and the lifetime τ that characterize this decay [80]. Many of the resonances at $f = 4$ thresholds have $a_{\rm res} < 100\ a_0$ and are likely to be difficult to observe in loss spectroscopy.

Resonances due to mechanism III are included in Tables IV and V. For ^{171}Yb, only three resonances meet the criteria for inclusion. For ^{173}Yb, there are none that meet the criteria, so we have included the widest undecayed resonance, at 553 G. Resonances due to mechanism III at excited thresholds are strongly decayed, with $a_{\rm res} < 10\ a_0$, as exemplified by the resonance at 113 G for Cs ($f = 3, m_f = 2$) interacting with ^{171}Yb. Such resonances are unlikely to be observable in three-body loss spectroscopy because $a(B)$ deviates so little from its background value.

There are several resonances in Tables IV and V for Cs ($f = 3$, $m_f = 3$) interacting with each of ^{173}Yb and ^{171}Yb. These resonances occur at fields where $\alpha_{\rm Cs}$ is large, so that experiments in an optical trap are likely to be hampered by fast intraspecies 3-body losses. However, they would be good candidates for magnetoassociation in an optical lattice. The strongest resonances in this category are those at 148 G for ^{171}Yb and at 620 and 700 G for ^{173}Yb.

Cs atoms in magnetically excited states offer additional possibilities. Promising candidates for observation in loss spectroscopy include those near 202 and 423 G for ^{171}Yb and those near 165, 720, and 1004 G for ^{173}Yb. The resonance near 165 G for $m_f = 2$ has a width similar to that near 168 G for $m_f = 3$, but $\alpha_{\rm Cs}$ is much smaller, corresponding to much slower three-body loss; the two-body loss rate $k_{2,\rm Cs}$ is also very small [72].

It should be noted that the resonances for Cs + ^{173}Yb have very small background scattering lengths, typically around 1 a_0. Because of this, the widths Δ as conventionally

TABLE IV. Experimentally promising resonances in ultracold collisions between Cs and ^{171}Yb. Parameters are given for the widest resonance in each set, and the corresponding value of $m_{i,\mathrm{Yb}}$ is given.

(f, m_f)	$m_{i,\mathrm{Yb}}$	$(\Delta f, \Delta m_f)$	Mechanism	B_{res} (G)	$\bar{\Delta}$ (mG)	a_{res} (a_0)	τ (s)	α_{Cs} (a_0)	$k_{2,\mathrm{Cs}}$ (cm^3 s^{-1})
(3, 3)	−1/2	(0, −1)	II	75	0.0048	1.7×10^8	9.7×10^4	1.36×10^3	
(3, 3)	−1/2	(1, 1)	III	81	0.0063	6.0×10^5	37	1.42×10^3	
(3, 3)	1/2	(1, 1)	II	149	0.33	1.1×10^{12}	1.2×10^6	1.82×10^3	
(3, 3)	1/2	(1, 0)	I + II	171	0.065	4.1×10^{11}	2.8×10^6	1.91×10^3	
(3, 2)	−1/2	(0, −1)	II	74	0.0081	1.6×10^8	5.6×10^4	2.08×10^3	7.36×10^{-13}
(3, 2)	−1/2	(1, 1)	III	113	0.0065	9.6	7.7×10^{-4}	-3.44×10^3	1.53×10^{-12}
(3, 2)	1/2	(1, 1)	II	203	0.34	9.5×10^2	1.4×10^{-3}	7.66×10^2	3.35×10^{-14}
(3, 2)	1/2	(1, 0)	I + II	247	0.18	9.9×10^2	3.4×10^{-3}	1.05×10^3	6.57×10^{-14}
(3, 2)	−1/2	(1, −1)	II	315	0.054	6.3×10^6	87	1.36×10^3	9.82×10^{-14}
(3, 2)	−1/2	(0, −1)	II	1517	0.057	2.1×10^5	17	1.64×10^3	5.55×10^{-14}
(3, 1)	−1/2	(0, −1)	II	74	0.0097	1.7×10^8	4.9×10^4	3.64×10^2	1.44×10^{-12}
(3, 1)	−1/2	(1, 1)	III	180	0.0074	3.3	3.6×10^{-4}	-2.47×10^3	8.27×10^{-12}
(3, 1)	1/2	(1, 1)	II	315	0.38	6.0×10^2	1.2×10^{-3}	-2.20×10^3	1.88×10^{-12}
(3, 1)	1/2	(1, 0)	I + II	423	0.44	6.2×10^2	1.3×10^{-3}	5.39×10^2	3.17×10^{-14}
(3, 1)	−1/2	(1, −1)	II	613	0.14	1.4×10^6	11	1.18×10^3	1.49×10^{-11}
(3, 1)	−1/2	(0, −1)	II	1373	0.069	2.5×10^5	14	-1.48×10^2	2.24×10^{-11}
(3, 0)	−1/2	(0, −1)	II	73	0.0097	1.8×10^8	5.0×10^4	-2.44×10^3	2.14×10^{-11}
(3, 0)	1/2	(1, 1)	II	613	0.46	1.4×10^3	3.3×10^{-3}	-2.03×10^3	1.01×10^{-11}
(3, 0)	1/2	(1, 0)	I + II	934	1.22	9.1×10^2	9.2×10^{-4}	6.77×10^2	9.23×10^{-12}
(3, 0)	−1/2	(0, −1)	II	1243	0.067	3.0×10^5	14	1.33×10^3	5.67×10^{-13}
(3, 0)	−1/2	(1, −1)	II	1444	0.14	2.3×10^5	1.9	1.49×10^2	1.53×10^{-11}
(3, −1)	−1/2	(0, −1)	II	73	0.0081	1.9×10^8	6.1×10^4	-8.35×10^3	5.31×10^{-11}
(3, −1)	−1/2	(0, −1)	II	1125	0.056	3.6×10^5	16	3.15×10^3	2.79×10^{-11}
(3, −1)	1/2	(1, 1)	II	1444	0.47	3.6×10^2	8.7×10^{-4}	8.12×10^3	2.43×10^{-11}
(3, −2)	−1/2	(0, −1)	II	73	0.0049	1.9×10^8	1.0×10^5	7.43×10^3	3.90×10^{-11}
(4, −4)	1/2	(0, 1)	II	72	0.0066	97	3.9×10^{-2}	2.95×10^3	2.49×10^{-11}
(4, −4)	1/2	(0, 1)	II	927	0.042	9.7×10^2	3.7×10^{-2}	2.94×10^3	2.39×10^{-11}
(4, −3)	1/2	(0, 1)	II	73	0.011	91	2.1×10^{-2}	1.10×10^3	1.92×10^{-10}
(4, −3)	1/2	(0, 1)	II	1021	0.075	2.4×10^2	6.3×10^{-3}	8.00×10^2	1.02×10^{-10}
(4, −2)	1/2	(0, 1)	II	73	0.015	78	1.4×10^{-2}	7.73×10^2	1.68×10^{-10}
(4, −2)	1/2	(0, 1)	II	1126	0.098	1.1×10^2	2.7×10^{-3}	6.16×10^2	7.59×10^{-11}
(4, −1)	1/2	(0, 1)	II	74	0.016	64	1.1×10^{-2}	6.68×10^2	1.54×10^{-10}
(4, −1)	1/2	(0, 1)	II	1243	0.11	58	1.6×10^{-3}	5.95×10^2	7.29×10^{-11}
(4, 0)	1/2	(0, 1)	II	74	0.016	50	8.4×10^{-3}	6.43×10^2	1.50×10^{-10}
(4, 0)	1/2	(0, 1)	II	1373	0.11	34	1.1×10^{-3}	6.46×10^2	8.18×10^{-11}
(4, 1)	1/2	(0, 1)	II	74	0.015	37	6.9×10^{-3}	6.77×10^2	1.55×10^{-10}
(4, 1)	1/2	(0, 1)	II	1517	0.098	20	9.2×10^{-4}	7.67×10^2	9.95×10^{-11}
(4, 2)	1/2	(0, 1)	II	75	0.011	24	5.8×10^{-3}	7.94×10^2	1.69×10^{-10}
(4, 2)	1/2	(0, 1)	II	1673	0.075	11	8.0×10^{-4}	1.00×10^3	1.23×10^{-10}
(4, 3)	1/2	(0, 1)	II	75	0.0066	12	5.0×10^{-3}	1.13×10^3	1.92×10^{-10}
(4, 3)	1/2	(0, 1)	II	1840	0.042	4.8	7.3×10^{-4}	1.51×10^3	1.39×10^{-10}

defined by Eq. (5) are much larger than the normalized widths $\bar{\Delta}$ given in Table V, typically by about two orders of magnitude.

V. CONCLUSION

We present a comprehensive theoretical study of magnetically tunable Feshbach resonances in ultracold collisions between Cs and Yb atoms. We carry out coupled-channel calculations of the complex scattering length and analyze the results to obtain resonance positions and widths. For resonances in collisions of Cs in magnetically excited states, we also extract parameters that characterize resonance decay and the lifetime of the molecular states responsible for the resonances.

We use an accurate interaction potential recently determined from photoassociation spectroscopy [43], which gives reliable scattering lengths for all isotopic combinations of Cs and Yb and gives accurate predictions for the energies of the molecular states that cause Feshbach resonances.

The resonances are driven by couplings due to spin-dependent terms in the Hamiltonian that vary with the internuclear distance. We carry out electronic structure calculations of the distance dependence of all the important spin-dependent interactions, including the scalar hyperfine, tensor hyperfine, nuclear electric quadrupole, and spin-rotation terms. The resulting couplings allow us to

TABLE V. Experimentally promising resonances in ultracold collisions between Cs and ^{173}Yb. Parameters are given for the widest resonance in each set, and the corresponding value of $m_{i,\mathrm{Yb}}$ is given.

(f, m_f)	$m_{i,\mathrm{Yb}}$	$(\Delta f, \Delta m_f)$	Mechanism	B_{res} (G)	$\bar{\Delta}$ (mG)	a_{res} (a_0)	τ (s)	α_{Cs} (a_0)	$k_{2,\mathrm{Cs}}$ (cm^3 s^{-1})
(3, 3)	−1/2	(0, −1)	II	167	0.011	2.7×10^{13}	7.1×10^{9}	1.90×10^{3}	
(3, 3)	−3/2	(1, 1)	III	553	0.0053	6.0×10^{8}	2.2×10^{4}	-2.02×10^{3}	
(3, 3)	1/2	(1, 1)	II	620	0.48	3.7×10^{7}	29	2.92×10^{3}	
(3, 3)	−5/2	(1, 0)	I + II	700	0.32	1.9×10^{13}	2.5×10^{7}	4.39×10^{3}	
(3, 2)	−1/2	(0, −1)	II	165	0.018	1.3×10^{9}	2.0×10^{5}	3.55×10^{2}	5.00×10^{-15}
(3, 2)	1/2	(1, 1)	II	804	0.49	7.5×10^{2}	7.1×10^{-4}	2.31×10^{3}	5.94×10^{-13}
(3, 2)	−5/2	(1, 0)	I + II	933	0.86	6.0×10^{5}	36	-6.08×10^{4}	3.49×10^{-12}
(3, 1)	−1/2	(0, −1)	II	163	0.022	8.5×10^{8}	1.1×10^{5}	-7.60×10^{3}	2.66×10^{-11}
(3, 1)	1/2	(1, 1)	II	1107	0.50	2.3×10^{2}	2.5×10^{-4}	1.41×10^{3}	6.63×10^{-13}
(3, 1)	−5/2	(1, 0)	I + II	1326	1.80	4.5×10^{5}	0.15	-1.65×10^{3}	1.32×10^{-11}
(3, 1)	−1/2	(1, −1)	II	1622	0.048	4.2×10^{8}	5.5×10^{3}	1.13×10^{3}	2.31×10^{-13}
(3, 0)	−1/2	(0, −1)	II	161	0.022	7.8×10^{8}	9.6×10^{4}	-9.88×10^{3}	1.08×10^{-10}
(3, 0)	1/2	(1, 1)	II	1624	0.52	88	1.1×10^{-4}	1.05×10^{3}	3.10×10^{-13}
(3, 0)	−1/2	(0, −1)	II	1815	0.13	3.5×10^{7}	1.0×10^{3}	2.15×10^{3}	2.14×10^{-12}
(3, 0)	−5/2	(1, 0)	I + II	1983	3.30	5.7×10^{5}	0.11	-2.63×10^{2}	2.22×10^{-10}
(3, −1)	−1/2	(0, −1)	II	159	0.018	8.5×10^{8}	1.2×10^{5}	6.95×10^{3}	5.15×10^{-11}
(3, −1)	−1/2	(0, −1)	II	1566	0.10	8.5×10^{8}	2.2×10^{4}	7.35×10^{4}	4.09×10^{-11}
(3, −2)	−1/2	(0, −1)	II	157	0.011	1.1×10^{9}	2.6×10^{5}	4.65×10^{3}	1.43×10^{-11}
(3, −2)	−1/2	(0, −1)	II	1357	0.058	2.1×10^{9}	7.0×10^{4}	1.33×10^{3}	2.46×10^{-13}
(3, −3)	−1/2	(1, −1)	II	1744	−0.30	1.0×10^{10}	1.8×10^{4}	9.43×10^{2}	1.34×10^{-13}
(4, −4)	−1/2	(0, 1)	II	157	0.015	37	6.3×10^{-3}	2.95×10^{3}	2.50×10^{-11}
(4, −4)	−1/2	(0, 1)	II	1188	0.069	36	7.2×10^{-4}	2.96×10^{3}	2.27×10^{-11}
(4, −3)	−1/2	(0, 1)	II	158	0.026	76	7.6×10^{-3}	1.01×10^{3}	1.52×10^{-10}
(4, −3)	−1/2	(0, 1)	II	1362	0.13	35	5.2×10^{-4}	7.37×10^{2}	9.39×10^{-11}
(4, −2)	−1/2	(0, 1)	II	160	0.033	1.1×10^{2}	8.5×10^{-3}	7.05×10^{2}	1.24×10^{-10}
(4, −2)	−1/2	(0, 1)	II	1574	0.17	27	4.3×10^{-4}	6.06×10^{2}	7.41×10^{-11}
(4, −1)	−1/2	(0, 1)	II	162	0.037	1.2×10^{2}	8.5×10^{-3}	6.07×10^{2}	1.10×10^{-10}
(4, −1)	−1/2	(0, 1)	II	1828	0.19	20	3.9×10^{-4}	6.26×10^{2}	7.82×10^{-11}
(4, 0)	−1/2	(0, 1)	II	165	0.037	1.0×10^{2}	7.7×10^{-3}	5.88×10^{2}	1.07×10^{-10}
(4, 1)	−1/2	(0, 1)	II	167	0.033	75	6.5×10^{-3}	6.27×10^{2}	1.13×10^{-10}
(4, 2)	−1/2	(0, 1)	II	169	0.026	47	5.3×10^{-3}	7.51×10^{2}	1.29×10^{-10}
(4, 3)	−1/2	(0, 1)	II	171	0.015	21	4.3×10^{-3}	1.10×10^{3}	1.56×10^{-10}

make quantitative predictions of resonance widths and other properties.

For bosonic isotopes of Yb, with zero nuclear spin, the resonances are driven almost entirely by the distance dependence of the scalar hyperfine interaction on Cs. The general features of the resulting resonances have been explored in previous work [34], but the much improved interaction potential used here allows us to make specific predictions of the resonance positions and widths for the first time.

For fermionic isotopes of Yb, with nonzero nuclear spin, there are several additional terms in the hyperfine Hamiltonian, including significant anisotropic terms that couple atomic and molecular states with different values of the partial-wave (or molecular rotation) quantum number L. The additional terms cause additional Feshbach resonances. They also split both the atomic and molecular states: The atomic states are split into regularly spaced Zeeman components, but the molecular states are split in more complicated ways, particularly for $L > 0$, and several different spin-dependent terms contribute. Each Feshbach resonance that would exist in the absence of these terms is split into a closely spaced set of resonances, spread over 1 G or less.

A particular feature of the fermionic systems is that bound states below one Cs $f = 3$ threshold can cause resonances at another $f = 3$ threshold with a different value of m_f. Because these states can be very weakly bound, they can cause resonances at relatively low field.

We have made a complete set of predictions for all Feshbach resonances below 5000 G for all isotopic combinations. We have identified resonances that are particularly promising for experimental investigation, both to detect resonances in an optical trap and to form molecules by magnetoassociation in an optical lattice.

The data presented in this work are available from Durham University [81].

ACKNOWLEDGMENTS

We are grateful to Florian Schreck for valuable discussions. This work was supported by the UK Engineering and Physical Sciences Research Council (EPSRC) Grants No. EP/I012044/1, No. EP/N007085/1, No. EP/P008275/1, and

No. EP/P01058X/1. J.A. acknowledges funding by the Spanish Ministry of Science and Innovation Grant No. CTQ2015-65033-P. P.S.Ż. acknowledges funding from National Science Center (NCN) Grant No. 2017/25/B/ST4/01486.

[1] C. Chin, R. Grimm, P. Julienne, and E. Tiesinga, Rev. Mod. Phys. **82**, 1225 (2010).
[2] K. E. Strecker, G. B. Partridge, and R. G. Hulet, Phys. Rev. Lett. **91**, 080406 (2003).
[3] S. Jochim, M. Bartenstein, A. Altmeyer, G. Hendl, C. Chin, J. H. Denschlag, and R. Grimm, Phys. Rev. Lett. **91**, 240402 (2003).
[4] J. Cubizolles, T. Bourdel, S. J. J. M. F. Kokkelmans, G. V. Shlyapnikov, and C. Salomon, Phys. Rev. Lett. **91**, 240401 (2003).
[5] K. Xu, T. Mukaiyama, J. R. Abo-Shaeer, J. K. Chin, D. E. Miller, and W. Ketterle, Phys. Rev. Lett. **91**, 210402 (2003).
[6] C. A. Regal, J. L. Bohn, C. Ticknor, and D. S. Jin, Nature (London) **424**, 47 (2003).
[7] E. A. Donley, N. R. Claussen, S. T. Thompson, and C. E. Wieman, Nature (London) **417**, 529 (2002).
[8] S. Dürr, T. Volz, A. Marte, and G. Rempe, Phys. Rev. Lett. **92**, 020406 (2004).
[9] J. Herbig, T. Kraemer, M. Mark, T. Weber, C. Chin, H.-C. Nägerl, and R. Grimm, Science **301**, 1510 (2003).
[10] M.-S. Heo, T. T. Wang, C. A. Christensen, T. M. Rvachov, D. A. Cotta, J.-H. Choi, Y.-R. Lee, and W. Ketterle, Phys. Rev. A **86**, 021602(R) (2012).
[11] T. Köhler, K. Góral, and P. S. Julienne, Rev. Mod. Phys. **78**, 1311 (2006).
[12] J. M. Hutson and P. Soldán, Int. Rev. Phys. Chem. **25**, 497 (2006).
[13] F. Lang, K. Winkler, C. Strauss, R. Grimm, and J. Hecker Denschlag, Phys. Rev. Lett. **101**, 133005 (2008).
[14] K.-K. Ni, S. Ospelkaus, M. H. G. de Miranda, A. Pe'er, B. Neyenhuis, J. J. Zirbel, S. Kotochigova, P. S. Julienne, D. S. Jin, and J. Ye, Science **322**, 231 (2008).
[15] J. G. Danzl, M. J. Mark, E. Haller, M. Gustavsson, R. Hart, J. Aldegunde, J. M. Hutson, and H.-C. Nägerl, Nat. Phys. **6**, 265 (2010).
[16] T. Takekoshi, L. Reichsöllner, A. Schindewolf, J. M. Hutson, C. R. Le Sueur, O. Dulieu, F. Ferlaino, R. Grimm, and H.-C. Nägerl, Phys. Rev. Lett. **113**, 205301 (2014).
[17] P. K. Molony, P. D. Gregory, Z. Ji, B. Lu, M. P. Köppinger, C. R. Le Sueur, C. L. Blackley, J. M. Hutson, and S. L. Cornish, Phys. Rev. Lett. **113**, 255301 (2014).
[18] J. W. Park, S. A. Will, and M. W. Zwierlein, Phys. Rev. Lett. **114**, 205302 (2015).
[19] M. Guo, B. Zhu, B. Lu, X. Ye, F. Wang, R. Vexiau, N. Bouloufa-Maafa, G. Quéméner, O. Dulieu, and D. Wang, Phys. Rev. Lett. **116**, 205303 (2016).
[20] T. M. Rvachov, H. Son, A. T. Sommer, S. Ebadi, J. J. Park, M. W. Zwierlein, W. Ketterle, and A. O. Jamison, Phys. Rev. Lett. **119**, 143001 (2017).
[21] L. D. Carr, D. DeMille, R. V. Krems, and J. Ye, New J. Phys. **11**, 055049 (2009).
[22] M. A. Baranov, M. Dalmonte, G. Pupillo, and P. Zoller, Chem. Rev. **112**, 5012 (2012).
[23] T. Lahaye, C. Menotti, L. Santos, M. Lewenstein, and T. Pfau, Rep. Prog. Phys. **72**, 126401 (2009).
[24] S. A. Moses, J. P. Covey, M. T. Miecnikowski, D. S. Jin, and J. Ye, Nat. Phys. **13**, 13 (2017).
[25] D. DeMille, Phys. Rev. Lett. **88**, 067901 (2002).
[26] J. A. Blackmore, L. Caldwell, P. D. Gregory, E. M. Bridge, R. Sawant, J. Aldegunde, J. Mur-Petit, D. Jaksch, J. M. Hutson, B. E. Sauer, M. R. Tarbutt, and S. L. Cornish, Quantum Sci. Technol. **4**, 014010 (2019).
[27] N. Nemitz, F. Baumer, F. Münchow, S. Tassy, and A. Görlitz, Phys. Rev. A **79**, 061403(R) (2009).
[28] F. Münchow, B. Cristian, M. Maximilian, and A. Görlitz, Phys. Chem. Chem. Phys. **13**, 18734 (2011).
[29] H. Hara, Y. Takasu, Y. Yamaoka, J. M. Doyle, and Y. Takahashi, Phys. Rev. Lett. **106**, 205304 (2011).
[30] V. V. Ivanov, A. Khramov, A. H. Hansen, W. H. Dowd, F. Münchow, A. O. Jamison, and S. Gupta, Phys. Rev. Lett. **106**, 153201 (2011).
[31] A. H. Hansen, A. Khramov, W. H. Dowd, A. O. Jamison, V. V. Ivanov, and S. Gupta, Phys. Rev. A **84**, 011606(R) (2011).
[32] P. S. Żuchowski, J. Aldegunde, and J. M. Hutson, Phys. Rev. Lett. **105**, 153201 (2010).
[33] D. A. Brue and J. M. Hutson, Phys. Rev. Lett. **108**, 043201 (2012).
[34] D. A. Brue and J. M. Hutson, Phys. Rev. A **87**, 052709 (2013).
[35] B. Pasquiou, A. Bayerle, S. M. Tzanova, S. Stellmer, J. Szczepkowski, M. Parigger, R. Grimm, and F. Schreck, Phys. Rev. A **88**, 023601 (2013).
[36] S. L. Kemp, K. L. Butler, R. Freytag, S. A. Hopkins, E. A. Hinds, M. R. Tarbutt, and S. L. Cornish, Rev. Sci. Instrum. **87**, 023105 (2016).
[37] S. A. Hopkins, K. Butler, A. Guttridge, S. Kemp, R. Freytag, E. A. Hinds, M. R. Tarbutt, and S. L. Cornish, Rev. Sci. Instrum. **87**, 043109 (2016).
[38] A. Guttridge, S. A. Hopkins, S. L. Kemp, M. D. Frye, J. M. Hutson, and S. L. Cornish, Phys. Rev. A **96**, 012704 (2017).
[39] A. Micheli, G. K. Brennen, and P. Zoller, Nat. Phys. **2**, 341 (2006).
[40] E. R. Meyer and J. L. Bohn, Phys. Rev. A **80**, 042508 (2009).
[41] V. Barbé, A. Ciamei, B. Pasquiou, L. Reichsöllner, F. Schreck, P. S. Żuchowski, and J. M. Hutson, Nat. Phys. **14**, 881 (2018).
[42] A. Guttridge, S. A. Hopkins, M. D. Frye, J. J. McFerran, J. M. Hutson, and S. L. Cornish, Phys. Rev. A **97**, 063414 (2018).
[43] A. Guttridge, M. D. Frye, B. C. Yang, J. M. Hutson, and S. L. Cornish, Phys. Rev. A **98**, 022707 (2018).
[44] See Supplemental Material at http://link.aps.org/supplemental/10.1103/PhysRevA.100.022704 for complete tables of parameters for all resonances at magnetic fields up to 5000 G for all isotopic combinations. The tables contain $B_{\rm res}$, $\bar{\Delta}$, Δ, $a_{\rm bg}$, and where appropriate $a_{\rm res}$, $\Gamma_B^{\rm inel}$ and τ, along with $\alpha_{\rm Cs}$ and $k_{2,\rm Cs}$, where it exists.

[45] E. Arimondo, M. Inguscio, and P. Violino, Rev. Mod. Phys. **49**, 31 (1977).

[46] L. Olschewski, Z. Phys. **249**, 205 (1972).

[47] J. Aldegunde and J. M. Hutson, Phys. Rev. A **97**, 042505 (2018).

[48] G. te Velde, F. M. Bickelhaupt, S. J. A. van Gisbergen, C. Fonseca Guerra, E. J. Baerends, J. G. Snijders, and T. Ziegler, J. Comput. Chem. **22**, 931 (2001).

[49] ADF2007.01, SCM, Theoretical Chemistry, Vrije Universiteit, Amsterdam, The Netherlands, 2007, http://www.scm.com.

[50] J. Aldegunde, B. A. Rivington, P. S. Żuchowski, and J. M. Hutson, Phys. Rev. A **78**, 033434 (2008).

[51] A. D. Becke, J. Chem. Phys. **98**, 5648 (1993).

[52] P. J. Stephens, F. J. Devlin, C. F. Chabalowski, and M. J. Frisch, J. Phys. Chem. **98**, 11623 (1994).

[53] A. Guttridge (unpublished).

[54] A. J. Moerdijk, B. J. Verhaar, and A. Axelsson, Phys. Rev. A **51**, 4852 (1995).

[55] F. H. Mies, E. Tiesinga, and P. S. Julienne, Phys. Rev. A **61**, 022721 (2000).

[56] P. S. Julienne, E. Tiesinga, and T. Köhler, J. Mod. Opt. **51**, 1787 (2004).

[57] G. F. Gribakin and V. V. Flambaum, Phys. Rev. A **48**, 546 (1993).

[58] N. Balakrishnan, V. Kharchenko, R. C. Forrey, and A. Dalgarno, Chem. Phys. Lett. **280**, 5 (1997).

[59] J. M. Hutson, New J. Phys. **9**, 152 (2007).

[60] M. D. Frye and J. M. Hutson, Phys. Rev. A **96**, 042705 (2017).

[61] In Cs, the large hyperfine splitting means that f remains a relatively good quantum number up to quite high fields, including most fields of experimental interest. However, lighter alkali-metal atoms have smaller hyperfine splittings so a different choice of labels may be appropriate.

[62] J. M. Hutson and C. R. Le Sueur, Comput. Phys. Commun. **241**, 1 (2019).

[63] J. M. Hutson and C. R. Le Sueur, MOLSCAT, BOUND, and FIELD, version 2019.0, 2019, https://github.com/molscat/molscat.

[64] J. M. Hutson and C. R. Le Sueur, Comput. Phys. Commun. **241**, 9 (2019).

[65] D. E. Manolopoulos, J. Chem. Phys. **85**, 6425 (1986).

[66] D. E. Manolopoulos, M. J. Jamieson, and A. D. Pradhan, J. Comput. Phys. **105**, 169 (1993).

[67] M. H. Alexander and D. E. Manolopoulos, J. Chem. Phys. **86**, 2044 (1987).

[68] J. M. Hutson, Comput. Phys. Commun. **84**, 1 (1994).

[69] B. Gao, Phys. Rev. A **62**, 050702(R) (2000).

[70] If the least-bound $L = 0$ state is sufficiently close to threshold, the associated $L = 2$ state may be above threshold and quasi-bound or unbound. According to AQDT [69], this will happen when the background s-wave scattering length is greater than $\bar{a}$, which is expected in about 50% of cases.

[71] M. Berninger, A. Zenesini, B. Huang, W. Harm, H.-C. Nägerl, F. Ferlaino, R. Grimm, P. S. Julienne, and J. M. Hutson, Phys. Rev. A **87**, 032517 (2013).

[72] M. D. Frye, B. C. Yang, and J. M. Hutson, Phys. Rev. A **100**, 022702 (2019).

[73] H.-W. Cho, D. J. McCarron, M. P. Köppinger, D. L. Jenkin, K. L. Butler, P. S. Julienne, C. L. Blackley, C. R. Le Sueur, J. M. Hutson, and S. L. Cornish, Phys. Rev. A **87**, 010703(R) (2013).

[74] M. Greiner, O. Mandel, T. Esslinger, T. W. Hänsch, and I. Bloch, Nature (London) **415**, 39 (2002).

[75] Where the two species have different trap frequencies, the relevant frequency is that of the confinement in the relative motion, $\omega_{\rm rel} = \sqrt{\omega_A^2 \mu/m_A + \omega_B^2 \mu/m_B}$ [82].

[76] M. Kitagawa, K. Enomoto, K. Kasa, Y. Takahashi, R. Ciuryło, P. Naidon, and P. S. Julienne, Phys. Rev. A **77**, 012719 (2008).

[77] T. Fukuhara, S. Sugawa, Y. Takasu, and Y. Takahashi, Phys. Rev. A **79**, 021601(R) (2009).

[78] T. Fukuhara, S. Sugawa, M. Sugimoto, S. Taie, and Y. Takahashi, Phys. Rev. A **79**, 041604(R) (2009).

[79] S. Sugawa, K. Inaba, S. Taie, R. Yamazaki, M. Yamashita, and Y. Takahashi, Nat. Phys. **7**, 642 (2011).

[80] For calculations at finite collision energy with $L_{\rm max} > 0$, there is always some scattering from $L = 0$ into the degenerate $L = 2$ channel, which results in finite $a_{\rm res}$ even when there are no truly inelastic open channels. In this case, $a_{\rm res}$ is nevertheless infinite at zero energy and the molecular lifetime is also infinite, even where the tables list large finite values arising from our calculations at $100\,{\rm nK} \times k_{\rm B}$.

[81] B. C. Yang, M. D. Frye, A. Guttridge, J. Aldegunde, P. S. Żuchowski, S. L. Cornish, and J. M. Hutson, Data for "Magnetic Feshbach resonances in ultracold collisions between Cs and Yb atoms", http://dx.doi.org/10.15128/r2mw22v546t (2019).

[82] F. Deuretzbacher, K. Plassmeier, D. Pfannkuche, F. Werner, C. Ospelkaus, S. Ospelkaus, K. Sengstock, and K. Bongs, Phys. Rev. A **77**, 032726 (2008).